

Simultaneously Transmitting and Reflecting Surface (STARS) for Terahertz Communications

Zhaolin Wang, *Graduate Student Member, IEEE*, Xidong Mu, *Member, IEEE*,
Jiaqi Xu, *Graduate Student Member, IEEE*, and Yuanwei Liu, *Senior Member, IEEE*

Abstract—A simultaneously transmitting and reflecting surface (STARS) aided terahertz (THz) communication system is proposed. A novel *power consumption model* depending on the type and the resolution of individual elements is proposed for the STARS. Then, the system energy efficiency (EE) and spectral efficiency (SE) are maximized in both narrowband and wideband THz systems. 1) For the narrowband system, an iterative algorithm based on penalty dual decomposition is proposed to jointly optimize the hybrid beamforming at the base station (BS) and the independent phase-shift coefficients at the STARS. The proposed algorithm is then extended to the coupled phase-shift STARS. 2) For the wideband system, to eliminate the beam split effect, a time-delay (TD) network implemented by the true-time-delayers is applied in the hybrid beamforming structure. An iterative algorithm based on the quasi-Newton method is proposed to design the coefficients of the TD network. Finally, our numerical results reveal that i) there is a slight performance loss of EE and SE caused by coupled phase shifts of the STARS in both narrowband and wideband systems, and ii) the conventional hybrid beamforming achieved close performance of EE and SE to the full-digital one in the narrowband system, but not in the wideband system where the TD-based hybrid beamforming is more efficient.

Index Terms—Beamforming design, simultaneously transmitting and reflecting surface, terahertz communications.

I. INTRODUCTION

The sixth generation (6G) wireless communication systems are expected to support at least one terabit per second (Tbps) peak data rate to enable emerging applications, such as virtual reality, vehicle-to-everything, Internet of Things, and Metaverse [1]. To this end, the communication over the terahertz (THz) band, which is located in the frequency range 0.1 THz–10 THz, has been regarded as a promising technique in 6G, since it is capable of providing a huge communication bandwidth in the order of tens of gigahertz (GHz) [2], [3]. Nevertheless, due to the very high frequency, the THz signals may suffer from significant propagation pass loss, which limits the communication distance. As such, the massive multiple-input multiple-output (MIMO) technique is the key enabler of THz communication [3]. In particular, thanks to the extremely small wavelength of THz signals, the ultra-massive antenna array can be constructed, which is capable of generating fine beams to compensate for significant pass loss in the THz band.

Simultaneous transmitting and reflecting surface (STARS) is another promising technique for 6G. Unlike the conventional

reconfigurable intelligent surface (RIS) that can only reflect the incident signal and thus lead to the *half-space* coverage [4], the STARS can simultaneously transmit and reflect the incident signal into both sides of the surface, resulting in the *full-space* coverage [5], [6]. As a result, STARS provides more degrees of freedom for manipulating the signal propagation and thereby enhances the design flexibility of the wireless network.

A. Prior Works

As aforementioned above, the massive MIMO technique plays a key role in THz communications, which can realize accurate beamforming to combat severe path loss. However, unlike the sub-6 GHz communications, the full-digital beamforming architecture, where each antenna owns a dedicated radio frequency (RF) chain, becomes impractical in the high-frequency band, such as millimeter-wave (mmWave) and THz, due to its high cost and power consumption [7]. Therefore, the hybrid analog and digital beamforming architecture comprising only a few RF chains and numerous low-cost phase shifters (PSs) has been widely studied [8]–[12]. More specifically, the authors of [8] proposed a series of alternating minimization algorithms for the hybrid beamforming design, where the matching error between the hybrid beamforming and the optimal full-digital beamforming is minimized. The authors of [9] analyzed the minimum number of RF chains required to realize the full-digital beamforming and then conceived a heuristic hybrid beamforming design to approach the optimal full-digital performance. Furthermore, the hybrid beamforming was designed via the matrix decomposition in [10] and [11], resulting in relatively low complexity. As a further advance, to investigate the performance limit of the hybrid beamforming, a penalty-based algorithm with provable optimality was developed in [12].

Nevertheless, the above hybrid beamforming designs merely focused on narrowband systems and thereby cannot fulfill the requirements of THz communications with huge spectrum resources, which motivates the investigation of the hybrid beamforming design in THz wideband systems [13]–[16]. In particular, a two-stage wideband hybrid beamforming design was proposed in [13] for multi-carrier systems over frequency selective fading channels. To break through the connectivity limit imposed by the number of RF chains, the authors of [14] conceived a cluster-based hybrid beamforming design to serve multiple users in the same beam but with different subcarriers. However, the significant beam split effect in the wideband THz communications was not considered in [13], [14]. To

The authors are with the School of Electronic Engineering and Computer Science, Queen Mary University of London, London E1 4NS, U.K. (e-mail: zhaolin.wang@qmul.ac.uk, xidong.mu@qmul.ac.uk, jiaqi.xu@qmul.ac.uk, yuanwei.liu@qmul.ac.uk).

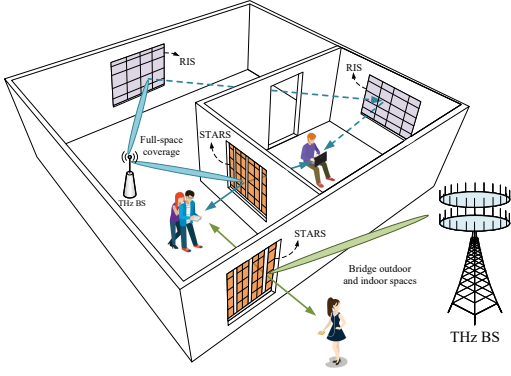


Fig. 1: Applications of STARS in THz communications.

combat the beam split effect, two hybrid beamforming designs based on virtual sub-array and true-time-delayers (TTDs), respectively, were proposed in [15]. As a further advance, the authors of [16] proposed a delay-phase beamforming design to eliminate the beam split effect, which was also implemented with the aid of TTDs.

Furthermore, due to the high obscuration susceptibility, THz communications may suffer from the problem of transmission unreliability caused by the blockage. The RIS is the possible solution to address this problem by establishing the additional line-of-sight (LOS) path, thus enhancing the performance of THz communications. The authors of [17] proposed a cooperative beam training scheme for RIS-aided THz communications and then designed the hybrid beamforming based on the training results. By considering the imperfect channel state information, a robust hybrid design was developed in [18] for RIS-aided THz communications. Furthermore, the authors of [19] propose to exploit the holographic RIS in THz communications to enhance the array gain. Most recently, the beam split effect in RIS-aided THz communications was investigated in [20].

B. Motivations and Contributions

Although the RIS provides possible solutions to solve the blockage problem in THz communications, its hardware limitation restricts its flexibility and effectiveness. More specifically, since the conventional RIS can only reflect the incident signals, the transmitter and receiver have to be located on the same side of the RIS. Therefore, multiple RISs may be required to overcome the blockage. For example, in indoor THz communications, as shown in Fig. 1, two conventional RISs are needed to serve the users in another room. As a remedy, the STARS is a promising technique to overcome the aforementioned limitations and thereby provide more benefits. On the one hand, it is more efficient to achieve full-space coverage by STARS. As illustrated in Fig. 1, the THz base station (BS) can cover the entire indoor space with the aid of only a single STARS. On the other hand, STARS is capable of bridging two disconnect spaces, such as indoor and outdoor spaces, which is impossible for the conventional RIS. Therefore, the STARS and THz communications can be

naturally linked together, which motivates us to exploit the STARS in THz communications.

To exploit the full potential of the STARS, in this paper, we propose the joint design of hybrid beamforming and STARS coefficients for both narrow and wideband THz communications. The primary contributions of this work are summarized as follows:

- We propose a novel STARS-aided THz communication system. To investigate the energy efficiency (EE) of the proposed system, we propose a novel power consumption model depending on the type and the resolution of individual elements for STARSs. In addition, we analyze the THz channels in both narrowband and wideband systems. Based on the unique characteristics of the THz channels in these two systems, we study the corresponding joint designs of hybrid beamforming and STARS coefficients.
- For the narrow system, we formulate a general EE and spectral efficiency (SE) maximization problem for hybrid beamforming and STARS coefficients. Then, considering the independent phase-shift STARS, we propose a double-loop iterative algorithm by exploiting the penalty dual decomposition (PDD) framework [21] to solve the formulated optimization problem. Furthermore, we extend the proposed algorithm to the cases with the coupled phase-shift STARS.
- For the wideband system, to mitigate the beam split effect, we introduce a time-delay (TD) network implemented by the TTDs into the hybrid beamforming. To optimize the coefficient of each TTD, we propose an iterative algorithm based on the quasi-Newton method.
- Our numerical results unveil that 1) the performance loss caused by the coupled phase shifts of STARSs is slight compared with the independent ones in both narrowband and wideband systems; 2) in the narrowband system, the performance of the hybrid beamforming with STARS is close to the full-digital one; and 3) in the wideband system, the TD-based hybrid beamforming with STARS achieves comparable performance as the full-digital one, while the conventional hybrid beamforming causes significant perform loss.

C. Organization and Notations

The rest of this paper is organized as follows. In Section II, the system model of the proposed STARS-aided THz communication system is presented. Then, the joint designs of hybrid beamforming and STARS coefficients for both narrowband and wideband systems are investigated in Sections III and IV, respectively. Section V provides numerical results to verify the effectiveness of the proposed designs. Finally, Section VI concludes the paper.

Notations: Scalars, vectors, and matrices are denoted by the lower-case, bold-face lower-case, and bold-face upper-case letters, respectively; $\mathbb{C}^{N \times M}$ denotes the space of $N \times M$ complex matrices; a^* and $|a|$ denote the conjugate and the magnitude of scalar a , respectively; $(\cdot)^T$, $(\cdot)^H$, $\|\cdot\|_F$, $\|\cdot\|_p$, and $\text{tr}(\cdot)$ denote the transpose, conjugate transpose, Frobenius norm, p -norm, and trace respectively; $\text{blkdiag}(\mathbf{A})$ denotes

a block diagonal matrix in which the diagonal blocks are the columns of \mathbf{A} ; \mathbf{I}_N denotes the $N \times N$ identity matrix; $[\mathbf{A}]_{i,j}$ denotes the element of the matrix \mathbf{A} at the i -th row and j -th column; $[\mathbf{a}]_{i:j}$ denotes the vector composed of the i -th to the j -th element of the vector \mathbf{a} ; $\mathbb{E}[\cdot]$ denotes the statistical expectation; $\text{Re}\{\cdot\}$ denotes the real component of a complex number; $\mathcal{CN}(\mu, \sigma^2)$ denotes the distribution of a circularly symmetric complex Gaussian (CSCG) random variable with mean μ and variance σ^2 ; $\mathcal{U}(a, b)$ denotes the uniform distribution between a and b ; $\Psi \setminus \Phi$ denotes difference set between Ψ and Φ .

II. SYSTEM MODEL

We consider a STARS-aided THz communication system, which consists of an N -antenna BS, an M -element STARS, and K single-antenna users whose indices are collected in \mathcal{K} . Without loss of generality, we assume that the users in subset $\mathcal{K}_t = \{1, \dots, K_0\}$ are located on the transmission side, and the users in subset $\mathcal{K}_r = \{K_0 + 1, \dots, K\}$ are located on the reflection side. The direct link between the BS and users are assumed to be blocked.

A. Signal Model for STARSs

The STARS elements excited by the incident signal are capable of radiating signals into both transmission and reflection spaces, which are referred to as transmitted signal and reflected signal, respectively. Let $s_m \in \mathbb{C}$ denote the incident signal at the m -th element. Then, the corresponding transmitted signal $t_m \in \mathbb{C}$ and reflected signal $r_m \in \mathbb{C}$ is given by [22]

$$t_m = \beta_{t,m} e^{j\phi_{t,m}} s_m, \quad r_m = \beta_{r,m} e^{j\phi_{r,m}} s_m, \quad (1)$$

where $\beta_{t,m}, \beta_{r,m} \in [0, 1]$ are the amplitude coefficients for transmission and reflection and $\phi_{t,m}, \phi_{r,m} \in [0, 2\pi]$ are the corresponding phase shifts introduced by the m -th elements. In this paper, we consider both independent and coupled phase-shift models for the STARS. In particular, for independent phase-shift STARSs, the law of energy conservation needs to be satisfied, which is given by

$$\beta_{t,m}^2 + \beta_{r,m}^2 \leq 1, \forall m \in \mathcal{M}, \quad (2)$$

where $\mathcal{M} = \{1, \dots, M\}$. Moreover, the phase shifts for transmission and reflection can be independently adjusted. However, the active or lossy elements are required to achieve independent control of the phase shifts, which can significantly increase manufacturing costs. As such, it is necessary to consider using passive lossless elements for STARSs, where the sum of the power of the transmitted and reflected signal should be equal to the power of the incident signal, i.e., the equality in (2) should be achieved and the electric and magnetic impedances of each element should be purely imaginary. Under such conditions, according to the analysis in [23], the transmission and reflection phase shifts of STARSs are coupled, leading to the following constraints:

$$\beta_{t,m}^2 + \beta_{r,m}^2 = 1, \forall m \in \mathcal{M}, \quad (3a)$$

$$\cos(\phi_{t,m} - \phi_{r,m}) = 0, \forall m \in \mathcal{M}. \quad (3b)$$

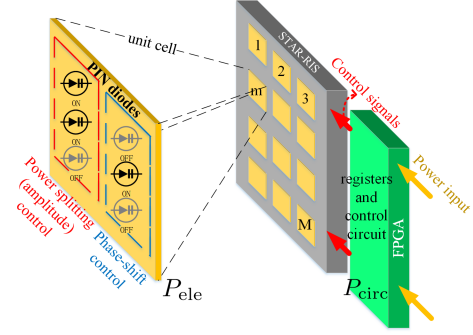


Fig. 2: Hardware structure of the STARS

The above two constraints are more complicated and challenging to address. Thus, in the sequel, we first focus on the independent phase-shift STARSs and then extend our design to the coupled phase-shift STARSs.

B. Proposed Power Consumption Model for STARSs

In this work, we consider patch-array-based STARSs [24] where the elements can accommodate positive-intrinsic-negative (PIN) diodes to configure the different states of the STARS element, as illustrated in Fig. 2. The power consumption of the STARS is composed of two parts, the static power consumption of the control circuit (e.g., field-programmable gate array (FPGA) board connected to the PIN diodes) and the dynamic power consumption of the STARS elements [25]. In principle, the static power consumption (P_{circ}) is independent of the operating states of the STAR elements. On the contrary, the dynamic power consumption (P_{ele}) depends on the different states of the element as well as the number of quantization levels of each element. In the following, we present the power consumption models for both independent phase-shift and coupled phase-shift STARSs.

1) *Independent Phase-shift STARSs*: Independent phase-shift STARSs are only subject to the energy conservation constraint as given in (2). Thus, as shown in Fig. 2, we need three sets of PIN diodes to control the power splitting ratio ($\beta_{t,m}/\beta_{r,m}$), the transmission phase-shift ($\phi_{t,m}$), and the reflection phase-shift ($\phi_{r,m}$), respectively. If the number of quantization levels assigned for the power splitting ratio and phase shifts are L_β and L_ϕ , respectively, then, the total number of PIN diodes required is $\lceil \log_2 L_\beta + 2 \log_2 L_\phi \rceil$, where $\lceil x \rceil$ is the ceiling function. As a result, we formulate the power consumption of the independent phase-shift STARS as follows:

$$P_{\text{STAR}}^i = M \cdot \frac{1}{2} \lceil \log_2 L_\beta + 2 \log_2 L_\phi \rceil \cdot P_{\text{PIN}} + P_{\text{circ}}, \quad (4)$$

where $\frac{1}{2} \lceil \log_2 L_\beta + 2 \log_2 L_\phi \rceil$ is the average number of PIN diodes in the “ON” state per element, $P_{\text{PIN}} \approx 0.33$ mW is the power consumption per PIN diode, and $P_{\text{circ}} \approx 10$ W for a large aperture surface [25].

2) *Coupled Phase-shift STARSs*: Coupled phase-shift STARSs are subject to the energy conservation constraint and the coupled phase-shift constraint in (3). Thus, for each element, we need two sets of PIN diodes to control the power

splitting and phase-shift for $\phi_{t,m}$, as well as an auxiliary PIN diode to determine whether $\phi_{t,m} - \phi_{r,m}$ is $\pi/2$ or $3\pi/2$ [23]. This is to say that for coupled phase-shift STARSs, the total number of PIN diodes required is $\lceil \log_2 L_\beta + \log_2 L_\phi + 1 \rceil$. As a result, we formulate the power consumption of coupled phase-shift STARSs as follows:

$$P_{\text{STAR}}^c = M \cdot \frac{1}{2} \lceil \log_2 L_\beta + \log_2 L_\phi + 1 \rceil \cdot P_{\text{PIN}} + P_{\text{circ}}, \quad (5)$$

Theoretically, to achieve the ideal case of continuous phase shifts, an infinite number of states are required. However, in practical cases, continuous phase shifts are obtained with tolerable phase-shift errors. For example, we consider the maximum tolerable error to be 1° , then the corresponding “continuous phase-shift” can be achieved with $\lceil \log_2 180 \rceil = 8$ PIN diodes per element. A similar result holds for the control bits of power splitting amplitudes.

C. THz Channel Model

In this work, we adopt the widely used ray-tracing-based channel model for THz communication. Generally, the THz communication channel consists of a line-of-sight (LOS) ray/path and a few non-LOS (NLOS) rays/paths. Denote L and L_k as the number of resolvable paths from the BS to the STARS and from the STARS to the user k , respectively. Then, the delay- q discrete-time baseband channel vector $\mathbf{h}_{i,j}^k[q] \in \mathbb{C}^{1 \times N}$ through the i -th BS-STARS path and the j -th STARS-user- k , $\forall k \in \mathcal{K}_i$ path is given by [26]–[28]

$$\mathbf{h}_{i,j}^k[q] = \alpha_i \tilde{\alpha}_{k,j} G_r G_t \text{sinc}(q - W(\tau_i + \tau_{k,j})) \mathbf{a}^H(f, \theta_{k,j}^h, \theta_{k,j}^v) \times \mathbf{\Theta}_i \mathbf{a}(f, \varphi_\ell^h, \varphi_\ell^v) \mathbf{b}^H(f, \tilde{\phi}_\ell), \quad (6)$$

where $\alpha_i = \sqrt{L^{-1}(f, D_i)} \bar{\alpha}_i$ with $L(f, D_i) \in \mathbb{R}$ and $\bar{\alpha}_i \in \mathbb{C}$ denoting the pathloss and complex coefficient of the i -th BS-STARS path, respectively, $\tilde{\alpha}_{k,j} = \sqrt{L^{-1}(f, \tilde{D}_{k,j})} \tilde{\alpha}_{k,j}$ with $L(f, \tilde{D}_{k,j}) \in \mathbb{R}$ and $\tilde{\alpha}_{k,j} \in \mathbb{C}$ denoting the pathloss and complex coefficient of the j -th STARS-user- k path, respectively, G_t and G_r are the antenna gain at the BS and user, respectively, $\text{sinc}(t) = \frac{\sin(\pi t)}{\pi t}$ is the pulse-shaping function, $W \in \mathbb{R}$ is the system bandwidth, $\tau_i, \tau_{k,j} \in \mathbb{R}$ are time delays of the i -th BS-STARS path and the j -th STARS-user- k path, respectively, f is the carrier frequency, and $\mathbf{\Theta}_i = \text{diag}([\beta_{i,1} e^{j\phi_{i,1}}, \dots, \beta_{i,M} e^{j\phi_{i,M}}]^T)$, $\forall i \in \{t, r\}$, denotes the transmission/reflection coefficient matrix of the STARS. We assume that the STARS is equipped with a $M_h \times M_v$ uniform planar array (UPA), where $M = M_h M_v$, and the BS is equipped with a uniform linear array (ULA). As such, the array response vector for the UPA at the STARS at the azimuth angle of θ_h and the elevation angle of θ_v can be modeled as

$$\begin{aligned} \mathbf{a}(f, \theta_h, \theta_v) &= [1, e^{j2\pi \frac{f}{c} d \sin \theta_h \sin \theta_v}, \dots, e^{j2\pi \frac{f}{c} (M_h-1) d \sin \theta_h \sin \theta_v}]^T \\ &\otimes [1, e^{j2\pi \frac{f}{c} d \cos \theta_v}, \dots, e^{-j2\pi \frac{f}{c} (M_v-1) d \cos \theta_v}]^T, \quad (7) \end{aligned}$$

where c is the speed of light and d is the antenna spacing. Furthermore, the array response vector for the ULA at the BS

at the azimuth angle of θ_h is given by

$$\mathbf{b}(f, \theta_h) = [1, e^{j2\pi \frac{f}{c} d \sin \theta_h}, \dots, e^{j2\pi \frac{f}{c} (N-1) d \sin \theta_h}]^T. \quad (8)$$

According to [29], the path loss $L(f, D)$ in the THz band includes both spreading loss and absorption loss, which is given by

$$\begin{aligned} L(f, D)[\text{dB}] &= L_{\text{spread}}(f, D)[\text{dB}] + L_{\text{absorption}}(f, D)[\text{dB}] \\ &= 20 \log_{10} \left(\frac{4\pi f D}{c} \right) + k(f) D 10 \log_{10} e. \quad (9) \end{aligned}$$

Here, D denotes the path length and $k(f)$ is the frequency-dependent medium absorption coefficient.

Furthermore, for each user k , we set the time of the first arrival path as the reference time, i.e., $\min_{i,j}(\tau_i + \tau_{k,j}) = 0$. Then, the delay spread of user k is $\tau_{d,k} = \max_{i,j}(\tau_i + \tau_{k,j})$. The overall channel $\bar{\mathbf{h}}_k[n]$ for user k at time index n is given by

$$\bar{\mathbf{h}}_k[n] = \sum_{q=0}^{Q_k-1} \sum_{j=1}^{L_k} \sum_{i=1}^L \mathbf{h}_{i,j}^k[q] \delta[n-q], \quad (10)$$

where Q_k denotes the maximum resolvable delays at user k and $\delta[\cdot]$ denotes the unit impulse function. The value of Q_k is determined by the delay spread $\tau_{d,k}$. In the following, we further analyze the overall channel $\bar{\mathbf{h}}_k[n]$ in the narrowband and wideband systems.

1) *Narrowband System:* In this case, we have $\tau_{d,k} \ll \frac{1}{W}$, $\forall k \in \mathcal{K}$ [26]. It follows that $W(\tau_i + \tau_{k,j}) \approx 0, \forall i, j$, leading to $\text{sinc}(q - W(\tau_i + \tau_{k,j})) \approx \text{sinc}(q), \forall i, j$. As such, due to the decay of the sinc function, we have $\mathbf{h}_{i,j}^k[q] \approx \mathbf{0}, \forall i, j$ when $q \geq 1$. In other words, all paths only contribute the most to the sampled received signal with a delay of 0. Therefore, in the narrowband STARS-aided THz communication system, the single delay-0 channel vector $\mathbf{h}_{i,j}^k[0]$ is sufficient to represent the overall channel, i.e., the channel is flat fading. Based on the above analysis, the overall channel $\bar{\mathbf{h}}_k[n] \in \mathbb{C}^{1 \times N}$ from the BS to the user k , $\forall k \in \mathcal{K}_i, \forall i \in \{t, r\}$ at the time index n reduces to

$$\begin{aligned} \bar{\mathbf{h}}_k[n] &\approx \sum_{j=1}^{L_k} \sum_{i=1}^L \mathbf{h}_{i,j}^k[0] \delta[n] \approx \left(G_r \sum_{j=1}^{L_k} \tilde{\alpha}_{k,j} \mathbf{a}^H(f, \theta_{k,j}^h, \theta_{k,j}^v) \right) \\ &\times \mathbf{\Theta}_i \left(G_t \sum_{i=1}^L \alpha_i \mathbf{a}(f, \varphi_\ell^h, \varphi_\ell^v) \mathbf{b}^H(f, \tilde{\phi}_\ell) \right) \delta[n]. \quad (11) \end{aligned}$$

2) *Wideband System:* In contrast to the narrowband system, the delay spread $\tau_{d,k}$ for user k can be comparable to or much larger than the sampling period $\frac{1}{W}$ in the wideband system. Therefore, each path may mainly contribute to different delays q , leading to $Q_k \geq 1$. Such a channel is referred to as a frequency-selective channel, which causes inter-symbol interference (ISI) since each user k receives overlapped transmit signals with different delays at each time index n . The multi-carrier orthogonal frequency-division multiplexing (OFDM) technique is typically exploited to tackle this problem, where the signal is transformed into the frequency domain using discrete Fourier transform (DFT). Denote M_c as the number of subcarriers in the OFDM system and f_c as the central

frequency. The frequency for the m -th subcarrier is thus given by $f_m = f_c + \frac{W(2m-1-M_c)}{2M_c}$. Then, the channel for user k on the m -th subcarrier obtained by DFT is given by

$$\bar{\mathbf{h}}_{m,k} = \sum_{q=0}^{Q_k-1} \sum_{j=1}^{L_k} \sum_{i=1}^L \mathbf{h}_{i,j}^k[f_m, q] e^{-\frac{j2\pi m q}{M_c}}, \forall m \in \mathcal{M}_c, \quad (12)$$

where $\mathcal{M}_c = \{1, \dots, M_c\}$. Note that in the above expression, we rephrase $\mathbf{h}_{i,j}^k[q]$ for the m -th subcarrier as $\mathbf{h}_{i,j}^k[f_m, q]$, since $\mathbf{h}_{i,j}^k[q]$ is also a function of carrier frequency, c.f., (6). To further explain this, we take the array response vector at the BS as an example. When manufacturing the antenna arrays, the antenna spacing is usually set as half of the wavelength at the central frequency, i.e., $d = \frac{c}{2f_c}$. Therefore, according to (8), the array response vector for the BS at the azimuth of θ_h at m -th subcarrier is given by

$$\mathbf{b}(f_m, \theta_h) = [1, e^{j\pi \frac{f_m}{f_c} \sin \theta_h}, \dots, e^{j\pi(N-1) \frac{f_m}{f_c} \sin \theta_h}]^T. \quad (13)$$

Define $\tilde{\theta}_{h,m} = \frac{f_m}{f_c} \sin \theta_h$ as the spatial direction at m -th subcarrier. It can be observed that although the physical direction θ_h is the same, the corresponding spatial direction $\tilde{\theta}_{h,m}$ for each subcarrier can be totally different, especially considering that the bandwidth W and the size of antenna array N can be very large in THz communication systems. As such, the frequency-domain channel $\bar{\mathbf{h}}_{m,k}, \forall m \in \mathcal{M}_c$ can be significantly *frequency-dependent*, which makes the system more challenging to design.

Therefore, in the following, we first investigate the narrowband system with simpler channel models. Then, we extend our design to the more completed wideband system. Moreover, we assume that the channels and the path angles have been obtained by the angle-based channel estimation method [30].

III. NARROWBAND SYSTEM

In this section, we investigate the simple narrowband STARS-aided wireless communication system with the hybrid beamforming structure for maximizing the EE and SE of the system. We first propose a PDD-based algorithm for solving the EE and SE maximization problem in the cases with the independent phase-shift STARS, which is then extended to the cases with the coupled phase-shift STARS.

A. Hybrid Beamforming

According to (9), the path loss in the THz band can be very large. In order to compensate for the severe path loss, a massive antenna array with a hybrid beamforming structure, as shown in Fig. 3, is typically used at the BS to achieve a large array gain. In the hybrid beamforming structure, we assume that there are N_{RF} RF chains ($N_{\text{RF}} \ll N$). Each RF chain is connected to the N antenna via N phase shifters (PSs). Therefore, there are total $N_{\text{RF}}N$ PSs. Denote $\mathbf{F}_{\text{RF}} \in \mathbb{C}^{N \times N_{\text{RF}}}$ as the analog beamformer achieved by PSs, $\mathbf{F}_{\text{BB}} = [\mathbf{f}_{\text{BB},1}, \dots, \mathbf{f}_{\text{BB},K}] \in \mathbb{C}^{N_{\text{RF}} \times K}$ as the digital beamformers for K users, and $\mathbf{s}[n] = [s_1[n], \dots, s_K[n]]^T \in \mathbb{C}^{K \times 1}$ as the information symbols for K users. The transmit signal at the BS is given by

$$\mathbf{x}[n] = \mathbf{F}_{\text{RF}} \mathbf{F}_{\text{BB}} \mathbf{s}[n] = \mathbf{F}_{\text{RF}} \sum_{k \in \mathcal{K}} \mathbf{f}_{\text{BB},k} s_k[n]. \quad (14)$$

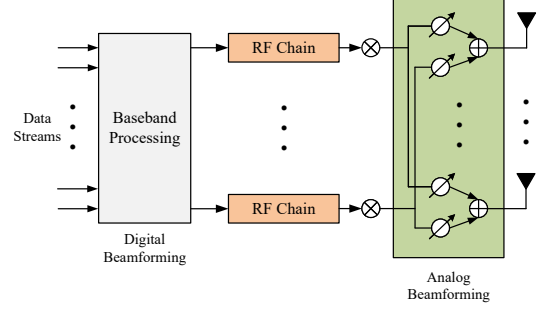


Fig. 3: Hybrid beamforming architecture at the BS.

Since the PSs can only change phase shifts of signals, the elements of the analog beamformer of \mathbf{F}_{RF} are constrained by

$$|[\mathbf{F}_{\text{RF}}]_{i,j}| = 1, \forall i = 1, \dots, N, j = 1, \dots, N_{\text{RF}}. \quad (15)$$

It is assumed that $\mathbf{s}[n]$ is the independent complex Gaussian signal, i.e., $\mathbb{E}[\mathbf{s}[n](\mathbf{s}[n])^H] = \mathbf{I}_K$. The covariance matrix of the transmit signal can be thus defined as $\mathbf{Q} = \mathbb{E}[\mathbf{x}[n](\mathbf{x}[n])^H] = \mathbf{F}_{\text{RF}} \mathbf{F}_{\text{BB}} \mathbf{F}_{\text{BB}}^H \mathbf{F}_{\text{RF}}^H$. In this paper, we consider the average power constraint, which is given by

$$\text{tr}(\mathbf{Q}) = \|\mathbf{F}_{\text{RF}} \mathbf{F}_{\text{BB}}\|_F^2 \leq P_t. \quad (16)$$

Then, the received signal at user $k, \forall k \in \mathcal{K}_i, \forall i \in \{t, r\}$, is given by

$$\begin{aligned} y_k[n] &= \bar{\mathbf{h}}_k[n] * \mathbf{x}[n] + n_k[n] \\ &= \mathbf{h}_k \boldsymbol{\Theta}_i \mathbf{G} \mathbf{F}_{\text{RF}} \sum_{k \in \mathcal{K}} \mathbf{f}_{\text{BB},k} s_k[n] + n_k[n] \\ &= \underbrace{\boldsymbol{\theta}_i^T \text{diag}(\mathbf{h}_k) \mathbf{G} \mathbf{F}_{\text{RF}} \mathbf{f}_{\text{BB},k} s_k[n]}_{\text{desired signal}} \\ &\quad + \underbrace{\sum_{j \in \mathcal{K}, j \neq k} \boldsymbol{\theta}_i^T \text{diag}(\mathbf{h}_k) \mathbf{G} \mathbf{F}_{\text{RF}} \mathbf{f}_{\text{BB},j} s_j[n]}_{\text{inter-user interference}} + n_k[n], \end{aligned} \quad (17)$$

where $\mathbf{h}_k = G_r \sum_{j=1}^{L_k} \tilde{\alpha}_{k,j} \mathbf{a}^H(f, \theta_{k,j}^h, \theta_{k,j}^v)$ denotes the overall STARS-user- k discrete-time baseband channel, $\mathbf{G} = G_t \sum_{i=1}^L \alpha_i \mathbf{a}(f, \varphi_i^h, \varphi_i^v) \mathbf{b}^H(f, \tilde{\phi}_i)$ denotes the overall BS-STARS discrete-time baseband channel, $\boldsymbol{\theta}_i = [\beta_{i,1} e^{j\phi_{i,1}}, \dots, \beta_{i,M}^{j\phi_{i,M}}]^T, \forall i \in \{t, r\}$, is the vector for STARS coefficients, and $n_k[n] \sim \mathcal{CN}(0, \sigma_k^2)$ is the additive complex Gaussian noise at user k . More particular, we have $\sigma_k^2 = \sigma_0^2 W$ with σ_0^2 denoting the noise power spectral density.

B. Problem Formulation

Energy efficiency (EE) is an important performance metric for THz communication, which is defined as the ratio of spectral efficiency (SE) in bit/s/Hz to power consumption in Watt (W). By defining $\mathbf{G}_k = \text{diag}(\mathbf{h}_k) \mathbf{G} \in \mathbb{C}^{M \times N}$, the achievable rate of user $k, \forall k \in \mathcal{K}_i, \forall i \in \{t, r\}$, can be obtained

according to (17) as follows:

$$R_k = \log_2 \left(1 + \frac{|\boldsymbol{\theta}_i^T \mathbf{G}_k \mathbf{F}_{\text{RF}} \mathbf{f}_{\text{BB},k}|^2}{\sum_{j \in \mathcal{K}, j \neq k} |\boldsymbol{\theta}_i^T \mathbf{G}_k \mathbf{F}_{\text{RF}} \mathbf{f}_{\text{BB},j}|^2 + \sigma_k^2} \right). \quad (18)$$

The system SE is the sum of the achievable rate of all users, which is given by

$$g(\boldsymbol{\chi}) = \sum_{k \in \mathcal{K}} R_k. \quad (19)$$

Here, $\boldsymbol{\chi} = \{\boldsymbol{\theta}_t, \boldsymbol{\theta}_r, \mathbf{F}_{\text{RF}}, \mathbf{F}_{\text{BB}}\}$. Then, to calculate the EE, we exploit a practical rate-dependent power consumption model as follows:

$$P(\boldsymbol{\chi}) = \|\mathbf{F}_{\text{RF}} \mathbf{F}_{\text{BB}}\|_F^2 + \xi g(\boldsymbol{\chi}) + P_c, \quad (20)$$

where $\|\mathbf{F}_{\text{RF}} \mathbf{F}_{\text{BB}}\|_F^2$ denotes the transmit power consumption, and ξ is a constant representing the dynamic power consumption per unit data rate (W/(bits/s/Hz)) caused by the coding, decoding, and backhaul processes [31], and P_c represents the rate-independent power consumption. More specifically, the rate-independent power consumption P_c is given by

$$P_c = P_{\text{BS}} + P_{\text{BB}} + N_{\text{RF}} P_{\text{RF}} + N_{\text{RF}} N P_{\text{PS}} + P_{\text{STAR}} + K P_{\text{UE}}, \quad (21)$$

where P_{BS} , P_{BB} , P_{RF} , P_{PS} , P_{STAR} , and P_{UE} denotes the power consumption for the oscillator and circuit at the BS, the baseband processing, each RF chain, each PS, the STARS, and the circuit at each user, respectively. More specifically, P_{STAR} is defined in (4) and (5) for independent phase-shift and coupled phase-shift STARSs, respectively. The system EE is thus given by

$$\eta(\boldsymbol{\chi}) = \frac{g(\boldsymbol{\chi})}{P(\boldsymbol{\chi})} = \frac{g(\boldsymbol{\chi})}{\|\mathbf{F}_{\text{RF}} \mathbf{F}_{\text{BB}}\|_F^2 + \xi g(\boldsymbol{\chi}) + P_c} \quad (22)$$

In this work, we aim to optimize the analog beamformer, digital beamformers, and STARS coefficients to maximize the EE, leading to the following optimization problem:

$$\max_{\boldsymbol{\chi}} \frac{g(\boldsymbol{\chi})}{\|\mathbf{F}_{\text{RF}} \mathbf{F}_{\text{BB}}\|_F^2 + \xi g(\boldsymbol{\chi}) + P_c} \quad (23a)$$

$$\text{s.t.} \quad (2) \text{ or } (3), \quad (23b)$$

$$\|\mathbf{F}_{\text{RF}} \mathbf{F}_{\text{BB}}\|_F^2 \leq P_t, \quad (23c)$$

$$|[\mathbf{F}_{\text{RF}}]_{i,j}| = 1, \forall i = 1, \dots, N, j = 1, \dots, N_{\text{RF}}, \quad (23d)$$

where constraint (23b) is the transmission and reflection coefficient constraint for the independent phase-shift STARS or the coupled phase-shift STARS, constraint (23c) is the total power constraint, and (23d) is imposed by the hardware limitation of PSs. We note that problem (23) becomes the SE maximization problem if the rate-dependent power consumption $\|\mathbf{F}_{\text{RF}} \mathbf{F}_{\text{BB}}\|_F^2 + \xi g(\boldsymbol{\chi})$ in the denominator of the objective function is omitted. This motivates us to formulate a general optimization problem for both EE and SE maximization as follows:

$$\max_{\boldsymbol{\chi}} \frac{g(\boldsymbol{\chi})}{w(\|\mathbf{F}_{\text{RF}} \mathbf{F}_{\text{BB}}\|_F^2 + \xi g(\boldsymbol{\chi})) + P_c} \quad (24a)$$

$$\text{s.t.} \quad (2) \text{ or } (3), (23c), (23d), \quad (24b)$$

where a factor w is introduced to control the rate-dependent power. In particular, The above problem reduces to the SE maximization problem when $w = 0$ and to the EE maximization problem when $w = 1$. This optimization problem is challenging to solve due to the non-convex fractional objective function, the coupling of $\boldsymbol{\theta}_i$, \mathbf{F}_{RF} , and \mathbf{F}_{BB} , and the constant modulus constraint (23d). Moreover, for coupled phase-shift STARSs, the equality constraint and coupled phase-shift constraint in (3) make the problem more complicated. Thus, in the following, we first propose a solution for the independent phase-shift STARS with constraint (2). Then, we extend the proposed solution to the coupled phase-shift STARS with constraint (3).

C. Proposed Solution for Independent Phase-shift STARSs

In this subsection, a PDD-based algorithm is proposed to solve problem (24) subject to constraint (2). Firstly, to transform the fractional objective function into a more tractable form, we introduce the auxiliary variables $\mathbf{r} = [r_1, \dots, r_K]^T$ for the rates $R_k, \forall k \in \mathcal{K}$, such that

$$r_k \leq R_k, \forall k \in \mathcal{K}, \quad (25)$$

and the auxiliary variables η , a , and b such that

$$\eta \leq \frac{a^2}{b}, \quad a^2 \leq \sum_{k \in \mathcal{K}} r_k, \quad (26)$$

$$w \left(\|\mathbf{F}_{\text{RF}} \mathbf{F}_{\text{BB}}\|_F^2 + \xi \sum_{k \in \mathcal{K}} r_k \right) + P_c \leq b. \quad (27)$$

Then, we have the following lemma.

Lemma 1. Problem (24) is equivalent to the following optimization problem:

$$\max_{\boldsymbol{\chi}, \mathbf{r}, \eta, a, b} \eta \quad (28a)$$

$$\text{s.t.} \quad \eta \leq \frac{a^2}{b}, \quad (28b)$$

$$a^2 \leq \sum_{k \in \mathcal{K}} r_k, \quad (28c)$$

$$w \left(\|\mathbf{F}_{\text{RF}} \mathbf{F}_{\text{BB}}\|_F^2 + \xi \sum_{k \in \mathcal{K}} r_k \right) + P_c \leq b, \quad (28d)$$

$$r_k \leq R_k, \forall k \in \mathcal{K}, \quad (28e)$$

$$(2) \text{ or } (3), (23c), (23d), \quad (28f)$$

Proof. According to constraints (28b)–(28d), it can be readily proved that maximizing η is equivalent to maximizing the following objective function:

$$\begin{aligned} \tilde{\eta} &= \frac{\sum_{k \in \mathcal{K}} r_k}{w(\|\mathbf{F}_{\text{RF}} \mathbf{F}_{\text{BB}}\|_F^2 + \xi \sum_{k \in \mathcal{K}} r_k) + P_c} \\ &= \left(\frac{w\|\mathbf{F}_{\text{RF}} \mathbf{F}_{\text{BB}}\|_F^2 + P_c}{\sum_{k \in \mathcal{K}} r_k} + w\xi \right)^{-1}. \end{aligned} \quad (29)$$

It can be seen that $\tilde{\eta}$ increases as $\sum_{k \in \mathcal{K}} r_k$ increase. Then, according to constraint (28e), we have the maximum value of

$\sum_{k \in \mathcal{K}} r_k$ is $\sum_{k \in \mathcal{K}} R_k = g(\chi)$. As such, the maximum value of $\tilde{\eta}$ must be the maximum value of the following function

$$\tilde{\eta} = \frac{g(\chi)}{w(\|\mathbf{F}_{\text{RF}}\mathbf{F}_{\text{BB}}\|_F^2 + \xi g(\chi)) + P_c}, \quad (30)$$

which is the objective function of problem (24). The proof is completed. ■

Based on **Lemma 1**, we focus on solving problem (28) with constraint (2) in the sequel. Next, to solve the coupling of θ_i , \mathbf{F}_{RF} , and \mathbf{F}_{BB} , we introduce the auxiliary variables $\mathbf{F} = [\mathbf{f}_1, \dots, \mathbf{f}_K] \in \mathbb{C}^{N \times K}$ such that

$$\mathbf{F} = \mathbf{F}_{\text{RF}}\mathbf{F}_{\text{BB}}, \quad (31)$$

and the auxiliary variables $\Xi = [\xi_1, \dots, \xi_K] \in \mathbb{C}^{K \times K}$ such that

$$\xi_{k,j} = \theta_i^T \mathbf{G}_k \mathbf{f}_j, \forall k \in \mathcal{K}_i, i \in \{t, r\}, j \in \mathcal{K}, \quad (32)$$

where $\xi_{k,j}$ denotes the j -th element of ξ_k . The equations in (32) can be reformulated more compactly as

$$\xi_k = \mathbf{F}^T \mathbf{G}_k^T \theta_i, \forall k \in \mathcal{K}_i, i \in \{t, r\}. \quad (33)$$

With these auxiliary variables, the achievable rate of user k can be rewritten as

$$R_k(\xi_k) = \log_2 \left(1 + \frac{|\xi_{k,k}|^2}{\sum_{j \in \mathcal{K}, j \neq k} |\xi_{k,j}|^2 + \sigma_k^2} \right). \quad (34)$$

Then, problem (28) with constraint (2) can be transformed into the following equivalent optimization problem:

$$\max_{\chi, \mathbf{F}, \Xi, \mathbf{r}, \eta, a, b} \quad \eta \quad (35a)$$

$$\text{s.t.} \quad \|\mathbf{F}\|_F^2 \leq P_t, \quad (35b)$$

$$w \left(\|\mathbf{F}\|_F^2 + \xi \sum_{k \in \mathcal{K}} r_k \right) + P_c \leq b, \quad (35c)$$

$$r_k \leq R_k(\xi_k), \forall k \in \mathcal{K}, \quad (35d)$$

$$\mathbf{F} = \mathbf{F}_{\text{RF}}\mathbf{F}_{\text{BB}}, \quad (35e)$$

$$\xi_k = \mathbf{F}^T \mathbf{G}_k^T \theta_i, \forall k \in \mathcal{K}_i, i \in \{t, r\}, \quad (35f)$$

$$(2), (23d), (28b), (28c). \quad (35g)$$

In the above optimization problem, all couplings are transformed into the equality constraints (35e) and (35f), which motivate us to exploit the PDD framework [21] to solve it. Specifically, by introducing the dual variables $\Psi \in \mathbb{C}^{N \times K}$ for constraint (35e) and $\lambda_k \in \mathbb{C}^{K \times 1}$, $\forall k \in \mathcal{K}$, for constraint (35f), the following augmented Lagrangian (AL) problem of problem (35) can be obtained:

$$\begin{aligned} \max_{\chi, \mathbf{F}, \Xi, \mathbf{r}, \eta, a, b} \quad & \eta - \frac{1}{2\rho} \|\mathbf{F} - \mathbf{F}_{\text{RF}}\mathbf{F}_{\text{BB}} + \rho\Psi\|_F^2 \\ & - \sum_{i \in \{t, r\}} \sum_{k \in \mathcal{K}_i} \frac{1}{2\rho} \|\xi_k - \mathbf{F}^T \mathbf{G}_k^T \theta_i + \rho\lambda_k\|_2^2 \end{aligned} \quad (36a)$$

$$\text{s.t.} \quad (2), (23d), (28b), (28c), (35b) - (35d), \quad (36b)$$

where $\rho \geq 0$ is the penalty factor. When $\rho \rightarrow +\infty$, the equality constraint can be achieved by solving the AL problem. The PDD framework has a double-loop structure. In the inner loop, the AL problem is solved. In the outer loop, the dual variables

and the penalty factor are updated according to the following policy [21]:

- Define the constraint violation function as

$$h = \max \left\{ \|\mathbf{F} - \mathbf{F}_{\text{RF}}\mathbf{F}_{\text{BB}}\|_\infty, \max_{k,i} \|\xi_k - \mathbf{F}^T \mathbf{G}_k^T \theta_i\|_\infty \right\}. \quad (37)$$

- If the constraint violation function $h(\chi, \mathbf{F}, \Xi)$ is smaller than the predefined threshold ε at the n -th iteration of the outer loop, the penalty factor keeps unchanged, while the dual variables are updated based on gradient descent as follows:

$$\Psi \leftarrow \Psi + \frac{1}{\rho} (\mathbf{F} - \mathbf{F}_{\text{RF}}\mathbf{F}_{\text{BB}}), \quad (38a)$$

$$\lambda_k \leftarrow \lambda_k + \frac{1}{\rho} (\xi_k - \mathbf{F}^T \mathbf{G}_k^T \theta_i), \forall k \in \mathcal{K}_i, i \in \{t, r\}. \quad (38b)$$

- If the constraint violation function is larger than the predefined threshold, the dual variables keep unchanged, and the penalty factor is updated by $\rho \leftarrow \kappa\rho$, where $0 < \kappa < 1$ is a reduction factor.

Therefore, in the following, we solve the AL problem (36) in the inner loop. We note that the AL problem is separable, which motivates us to solve it through the block coordinate descent (BCD). In particular, we divided the optimization variables into several blocks, namely $\{\mathbf{F}, \Xi, \mathbf{r}, \eta, a, b\}$, $\{\theta_t, \theta_r\}$, \mathbf{F}_{RF} , and \mathbf{F}_{BB} . In each iteration of the inner loop, each block is updated sequentially by fixing the other blocks, resulting in the following subproblems.

1) *Subproblem with respect to $\{\mathbf{F}, \Xi, \mathbf{r}, \eta, a, b\}$* : By fixing the other blocks, the subproblem with respect to $\{\mathbf{F}, \Xi, \mathbf{r}, \eta, a, b\}$ is given by

$$\begin{aligned} \max_{\mathbf{F}, \Xi, \mathbf{r}, \eta, a, b} \quad & \eta - \frac{1}{2\rho} \|\mathbf{F} - \mathbf{F}_{\text{RF}}\mathbf{F}_{\text{BB}} + \rho\Psi\|_F^2 \\ & - \sum_{i \in \{t, r\}} \sum_{k \in \mathcal{K}_i} \frac{1}{2\rho} \|\xi_k - \mathbf{F}^T \mathbf{G}_k^T \theta_i + \rho\lambda_k\|_2^2 \end{aligned} \quad (39a)$$

$$\text{s.t.} \quad (28b), (28c), (35b) - (35d). \quad (39b)$$

The non-convexity of this problem only lies in constraints (28b) and (35d). We observe that the right-hand side of the constraint (28b), i.e., a^2/b , is a quadratic-over-linear function, which is jointly convex for a and b . This motivates us to exploit SCA to approximate it. Given the point $(a^{[t]}, b^{[t]})$ obtained in the t -th iteration of the inner loop, the following affine lower bound of a^2/b can be obtained via the first-order Taylor expansion:

$$\frac{a^2}{b} \geq \frac{2a^{[t]}}{b^{[t]}} a - \left(\frac{a^{[t]}}{b^{[t]}} \right)^2 b \triangleq \varpi^{[t]}(a, b). \quad (40)$$

Now, we show that the constraint (35d) can be approximated in a similar way. By defining $\gamma_k \triangleq \frac{|\xi_{k,j}|^2}{\sum_{j \in \mathcal{K}, j \neq k} |\xi_{k,j}|^2 + \sigma_k^2}$, the constraint (35d) can be reformulated as

$$2^{r_k} - 1 \leq \gamma_k, \forall k \in \mathcal{K}. \quad (41)$$

The expression of γ_k is also in a quadratic-over-linear form. Therefore, by defining $I_k(\xi_k) \triangleq \sum_{j \in \mathcal{K}, j \neq k} |\xi_{k,j}|^2 + \sigma_k^2$, the

following affine lower bound of γ_k can be obtained based on the results in (40):

$$\gamma_k \geq \frac{2\text{Re}\left\{\left(\xi_{k,k}^{[t]}\right)^* \xi_{k,k}\right\}}{I_k(\xi_k^{[t]})} - \left|\frac{\xi_{k,k}^{[t]}}{I_k(\xi_k^{[t]})}\right|^2 I_k(\xi_k) \triangleq \bar{\gamma}_k^{[t]}(\xi_k). \quad (42)$$

As such, problem (39) can be approximated by the following optimization problem:

$$\max_{\mathbf{F}, \Xi, \mathbf{r}, \eta, a, b} \quad \eta - \frac{1}{2\rho} \|\mathbf{F} - \mathbf{F}_{\text{RF}}\mathbf{F}_{\text{BB}} + \rho\boldsymbol{\Psi}\|_F^2 - \sum_{i \in \{t, r\}} \sum_{k \in \mathcal{K}_i} \frac{1}{2\rho} \|\xi_k - \mathbf{F}^T \mathbf{G}_k^T \boldsymbol{\theta}_i + \rho\lambda_k\|_2^2 \quad (43a)$$

$$\text{s.t.} \quad \eta \leq \varpi^{[t]}(a, b) \quad (43b)$$

$$2^{r_k} - 1 \leq \bar{\gamma}_k^{[t]}(\xi_k), \forall k \in \mathcal{K}, \quad (43c)$$

$$(28c), (35b), (35c). \quad (43d)$$

The above optimization problem is convex and can be effectively solved by the standard interior-point algorithm.

2) *Subproblem with respect to $\{\boldsymbol{\theta}_t, \boldsymbol{\theta}_r\}$* : The block $\{\boldsymbol{\theta}_t, \boldsymbol{\theta}_r\}$ only appears in the last term of the objective function and the constraint (2). Thus, the corresponding subproblem is given by

$$\min_{\boldsymbol{\theta}_t, \boldsymbol{\theta}_r} \sum_{i \in \{t, r\}} \sum_{k \in \mathcal{K}_i} \|\xi_k - \mathbf{F}^T \mathbf{G}_k^T \boldsymbol{\theta}_i + \rho\lambda_k\|_2^2 \quad (44a)$$

$$\text{s.t.} \quad \beta_{t,m}^2 + \beta_{r,m}^2 \leq 1, \forall m \in \mathcal{M}, \quad (44b)$$

which is also convex and can be solved by the standard interior-point algorithm.

3) *Subproblem with respect to \mathbf{F}_{RF}* : The block \mathbf{F}_{RF} only contributes to the second term in the objective function and the constant modulus constraint (23d), leading to the following subproblem:

$$\min_{\mathbf{F}_{\text{RF}}} \|\mathbf{F} - \mathbf{F}_{\text{RF}}\mathbf{F}_{\text{BB}} + \rho\boldsymbol{\Psi}\|_F^2 \quad (45a)$$

$$\text{s.t.} \quad |[\mathbf{F}_{\text{RF}}]_{i,j}| = 1, \forall i = 1, \dots, N, j = 1, \dots, N_{\text{RF}}. \quad (45b)$$

The above subproblem can be simplified as

$$\min_{\mathbf{F}_{\text{RF}}} \text{tr}(\mathbf{F}_{\text{RF}}^H \mathbf{F}_{\text{RF}} \mathbf{A}) - 2\text{Re}\{\text{tr}(\mathbf{F}_{\text{RF}}^H \mathbf{B})\} \quad (46a)$$

$$\text{s.t.} \quad |[\mathbf{F}_{\text{RF}}]_{i,j}| = 1, \forall i = 1, \dots, N, j = 1, \dots, N_{\text{RF}}, \quad (46b)$$

where $\mathbf{A} = \mathbf{F}_{\text{BB}}\mathbf{F}_{\text{BB}}^H$ and $\mathbf{B} = (\mathbf{F} + \rho\boldsymbol{\Psi})\mathbf{F}_{\text{BB}}^H$. Note that the above problem is a quadratic optimization problem with separable unit modulus constraints. Furthermore, it can be readily known that the objective function of problem (46) can be reformulated as a quadratic function with respect to each element of \mathbf{F}_{RF} , which motivates us to exploit BCD to solve this problem. More specifically, each element of \mathbf{F}_{RF} is optimized at each iteration of BCD by fixing the other elements. Based on the above analysis, the subproblem with respect to the (i, j) -th element $[\mathbf{F}_{\text{RF}}]_{i,j}$ can be expressed as

$$\min_{|[\mathbf{F}_{\text{RF}}]_{i,j}|=1} p_{i,j} |[\mathbf{F}_{\text{RF}}]_{i,j}|^2 - \text{Re}\{q_{i,j}^* [\mathbf{F}_{\text{RF}}]_{i,j}\}, \quad (47)$$

where $p_{i,j}$ is some real coefficient and $q_{i,j}$ is some complex coefficient. Given that $|[\mathbf{F}_{\text{RF}}]_{i,j}| = 1$, it can be readily

Algorithm 1 BCD-based algorithm for solving problem (46).

```

1: initialize  $\mathbf{F}_{\text{RF}}$ , and set  $n = 0$ .
2: repeat
3:   for  $(i, j) \in \{1, \dots, N\} \times \{1, \dots, N_{\text{RF}}\}$  do
4:     calculate  $q_{i,j}$  according to (49).
5:     update  $[\mathbf{F}_{\text{RF}}]_{i,j}$  as  $q_{i,j}/|q_{i,j}|$ .
6:   end for
7: until the fractional reduction of the objective value falls
   below a predefined threshold.

```

obtained that the optimal solution to problem (47) is

$$[\mathbf{F}_{\text{RF}}]_{i,j} = \frac{q_{i,j}}{|q_{i,j}|}. \quad (48)$$

Thus, it is only needed to know the explicit expression of $q_{i,j}$. Following the path in [12, Appendix B], it can be shown that $q_{i,j}$ is given by

$$q_{i,j} = [\mathbf{F}_{\text{RF}}]_{i,j} [\mathbf{A}]_{j,j} - [\mathbf{F}_{\text{RF}} \mathbf{A}]_{i,j} + [\mathbf{B}]_{i,j}. \quad (49)$$

Therefore, problem (46) can be solved following the process in **Algorithm 1**.

4) *Subproblem with respect to \mathbf{F}_{BB}* : The subproblem with respect to \mathbf{F}_{BB} is given by

$$\min_{\mathbf{F}_{\text{BB}}} \|\mathbf{F} - \mathbf{F}_{\text{RF}}\mathbf{F}_{\text{BB}} + \rho\boldsymbol{\Psi}\|_F^2. \quad (50)$$

The above problem is an unconstrained convex optimization problem. Thus, the optimal solution can be obtained by the first-order optimality condition and is given by

$$\mathbf{F}_{\text{BB}}^* = (\mathbf{F}_{\text{RF}}^H \mathbf{F}_{\text{RF}})^{-1} \mathbf{F}_{\text{RF}}^H (\mathbf{F} + \rho\boldsymbol{\Psi}). \quad (51)$$

Based on the proposed solutions for the four subproblems, the AL problem (36) can be solved by updating the blocks $\{\mathbf{F}, \Xi, \mathbf{r}, \eta, a, b\}$, $\{\boldsymbol{\theta}_t, \boldsymbol{\theta}_r\}$, \mathbf{F}_{RF} , and \mathbf{F}_{BB} iteratively in the inner loop of the PDD framework. In the outer loop, the dual variables and the penalty factor are updated according to the aforementioned policy. The proposed PDD-based algorithm for problem (35) is summarized in **Algorithm 2**. The initial optimization variables are generated as follows. For the BS, the analog beamformer \mathbf{F}_{RF} is initialized based on the knowledge of the physical directions of the channel in (6). More specifically, the N_{RF} strongest paths are firstly selected from the total L paths between the BS and the STARS. The analog beamformer is then initialized to generate directional beams toward the physical directions of these paths. For example, for the ℓ -th strongest path with the physical direction $\tilde{\phi}_\ell$, the ℓ -th column $\mathbf{f}_{\text{RF},\ell}^{\text{init}}$ of the initial analog beamformer is given by

$$\mathbf{f}_{\text{RF},\ell}^{\text{init}} = \mathbf{b}(f, \tilde{\phi}_\ell). \quad (52)$$

Then, the digital beamformer \mathbf{F}_{BB} and the STARS coefficients $\{\boldsymbol{\theta}_t, \boldsymbol{\theta}_r\}$ are randomly initialized such that the constraint (23c) and the constraint (2) are satisfied, respectively. The auxiliary variables are initialized such that the corresponding equality constraints are satisfied.

The complexity of **Algorithm 2** mainly arises from the BCD iterations in the inner loop. Firstly, in each BCD iteration, the general complexity of solving problem (43)

Algorithm 2 PDD-based algorithm for solving problem (35).

```

1: initialize the optimization variables, and set  $0 < c < 1$ .
2: repeat
3:   repeat
4:     update  $\{\mathbf{F}, \Xi, \mathbf{r}, \eta, a, b\}$  by solving problem (43).
5:     update  $\{\boldsymbol{\theta}_t, \boldsymbol{\theta}_r\}$  by solving problem (44).
6:     update  $\mathbf{F}_{\text{RF}}$  by Algorithm 1.
7:     update  $\mathbf{F}_{\text{BB}}$  by (51).
8:   until convergence.
9:   if  $h \leq \varepsilon$  then
10:    update the dual variables  $\Psi$  and  $\{\lambda_k\}_{k \in \mathcal{K}}$  by (38).
11:   else
12:    update the penalty factor as  $\rho \leftarrow c\rho$ .
13:   end if
14:   set  $\varepsilon = 0.9h$ .
15: until  $h$  falls below a predefined threshold.

```

is dominated by the second-order cone (SOC) constraints. In problem (43), there are $P_{(43)} = NK + K^2 + K + 3$ optimization variables, K SOC constraints with the dimension of $K - 1$, and two SOC constraints with the dimension of NK . Thus, the complexity of solving problem (43) is $\mathcal{O}((P_{(43)})^3 + (P_{(43)})^2(K(K - 1)^2 + 2N^2K^2))$. Similarly, in problem (44), there are $2M$ optimization variables and M SOC constraints with the dimension of 2. Thus, the complexity of solving problem (44) is $\mathcal{O}(24M^3)$. Next, in each iteration of **Algorithm 1**, there are NN_{RF} closed-form solutions are calculated according to (49). The complexity of **Algorithm 1** is $\mathcal{O}(I_{\text{alg1}}NN_{\text{RF}})$, where I_{alg1} denotes the total number of iterations of **Algorithm 1**. Furthermore, the main complexity of calculating the closed-form \mathbf{F}_{BB} according to (51) arises from the matrix inversion operation, the complexity of which is $\mathcal{O}(N_{\text{RF}}^3)$.

D. Proposed Solution for Coupled Phase-shift STARSs

In this subsection, we extend the proposed PDD-based algorithm for the independent phase-shift STARS to the cases with the coupled phase-shift STARS by exploiting the general optimization framework developed in [32]. The difference between the optimization problems for independent and coupled phase-shift STARSs only falls in the constraints (2) and (3). The latter constraint is more complicated and non-convex. Following the path in [32], we can further introduce an additional equality constraint to solve the constraint (3), i.e.,

$$\tilde{\boldsymbol{\theta}}_i = \boldsymbol{\theta}_i, \forall i \in \{t, r\}, \quad (53)$$

where $\tilde{\boldsymbol{\theta}}_i = [\tilde{\beta}_{i,1}e^{j\tilde{\phi}_{i,1}}, \dots, \tilde{\beta}_{i,M}e^{j\tilde{\phi}_{i,M}}]^T, \forall i \in \{t, r\}$, is the auxiliary variable. Similar to problem (35), the transformed problem for coupled phase-shift STARSs is given by

$$\max_{\chi, \tilde{\boldsymbol{\theta}}_t, \tilde{\boldsymbol{\theta}}_r, \mathbf{F}, \Xi, \mathbf{r}, \eta, a, b} \quad \eta \quad (54a)$$

$$\text{s.t.} \quad \tilde{\boldsymbol{\theta}}_i = \boldsymbol{\theta}_i, \forall i \in \{t, r\}, \quad (54b)$$

$$\tilde{\beta}_{t,m}^2 + \tilde{\beta}_{r,m}^2 = 1, \forall m \in \mathcal{M}, \quad (54c)$$

$$\cos(\tilde{\phi}_{t,m} - \tilde{\phi}_{r,m}) = 0, \forall m \in \mathcal{M}, \quad (54d)$$

$$(23d), (28b), (28c), (35c) - (35f). \quad (54e)$$

In this problem, the original complicated constraint (3) is transferred to the auxiliary variables $\tilde{\boldsymbol{\theta}}_i, \forall i \in \{t, r\}$, and the optimization variables $\boldsymbol{\theta}_i, \forall i \in \{t, r\}$, is merely related to the equality constraint (54b). Then, we can obtain the following AL problem:

$$\begin{aligned} \max_{\chi, \tilde{\boldsymbol{\theta}}_t, \tilde{\boldsymbol{\theta}}_r, \mathbf{F}, \Xi, \mathbf{r}, \eta, a, b} \quad & \eta - \frac{1}{2\rho} \|\mathbf{F} - \mathbf{F}_{\text{RF}}\mathbf{F}_{\text{BB}} + \rho\Psi\|_F^2 \\ & - \sum_{i \in \{t, r\}} \sum_{k \in \mathcal{K}_i} \frac{1}{2\rho} \|\xi_k - \mathbf{F}^T \mathbf{G}_k^T \boldsymbol{\theta}_i + \rho\lambda_k\|_2^2 \\ & - \sum_{i \in \{t, r\}} \frac{1}{2\rho} \|\tilde{\boldsymbol{\theta}}_i - \boldsymbol{\theta}_i + \rho\tilde{\lambda}_i\|_2^2 \end{aligned} \quad (55a)$$

$$\text{s.t.} \quad (23d), (28b), (28c), (35c), (35d), (54c), (54d), \quad (55b)$$

where $\tilde{\lambda}_i \in \mathbb{C}^{M \times 1}, \forall i \in \{t, r\}$, are the dual variables for the constraint (54b). Similarly, the AL problem can be solved through BCD by dividing the optimization variables into blocks $\{\mathbf{F}, \Xi, \mathbf{r}, \eta, a, b\}$, $\{\boldsymbol{\theta}_t, \boldsymbol{\theta}_r\}$, $\{\tilde{\boldsymbol{\theta}}_t, \tilde{\boldsymbol{\theta}}_r\}$, \mathbf{F}_{RF} , and \mathbf{F}_{BB} . All blocks can be updated in the same way as the independent phase-shift STARS case, except $\{\boldsymbol{\theta}_t, \boldsymbol{\theta}_r\}$ and $\{\tilde{\boldsymbol{\theta}}_t, \tilde{\boldsymbol{\theta}}_r\}$. Therefore, we only focus on solving the subproblems with respect to these two blocks in the following.

1) *Subproblem with respect to $\{\boldsymbol{\theta}_t, \boldsymbol{\theta}_r\}$* : The block $\{\boldsymbol{\theta}_t, \boldsymbol{\theta}_r\}$ appears in the second and third terms of the objective function. The corresponding subproblem is thus given by

$$\begin{aligned} \min_{\boldsymbol{\theta}_t, \boldsymbol{\theta}_r} \quad & \sum_{i \in \{t, r\}} \sum_{k \in \mathcal{K}_i} \|\xi_k - \mathbf{F}^T \mathbf{G}_k^T \boldsymbol{\theta}_i + \rho\lambda_k\|_2^2 \\ & + \sum_{i \in \{t, r\}} \|\tilde{\boldsymbol{\theta}}_i - \boldsymbol{\theta}_i + \rho\tilde{\lambda}_i\|_2^2. \end{aligned} \quad (56)$$

With some algebraic manipulations, the above problem can be simplified as

$$\min_{\boldsymbol{\theta}_t, \boldsymbol{\theta}_r} \quad \sum_{i \in \{t, r\}} \left(\sum_{k \in \mathcal{K}_i} \|\Phi_k \boldsymbol{\theta}_i - \varsigma_k\|_2^2 + \|\boldsymbol{\theta}_i - \tilde{\varsigma}_i\|_2^2 \right), \quad (57)$$

where $\Phi_k = \mathbf{F}^T \mathbf{G}_k^T$, $\lambda_k = [\lambda_{k,1}, \dots, \lambda_{k,K}]^T$, $\varsigma_k = \xi_k + \rho\lambda_k$, and $\tilde{\varsigma}_i = \tilde{\boldsymbol{\theta}}_i + \rho\tilde{\lambda}_i$. This problem is an unconstrained convex optimization problem. Thus, the optimal solution can be obtained by checking the first-order optimality condition, which is given by

$$\boldsymbol{\theta}_i^* = \left(\sum_{k \in \mathcal{K}_i} \Phi_k^H \Phi_k + \mathbf{I}_M \right)^{-1} \left(\sum_{k \in \mathcal{K}_i} \Phi_k^H \varsigma_k + \tilde{\varsigma}_i \right), \quad \forall i \in \{t, r\}. \quad (58)$$

2) *Subproblem with respect to $\{\tilde{\boldsymbol{\theta}}_t, \tilde{\boldsymbol{\theta}}_r\}$* : The block $\{\tilde{\boldsymbol{\theta}}_t, \tilde{\boldsymbol{\theta}}_r\}$ is only related to the second term of the objective function and the constraints (54c) and (54d). Thus, the subproblem with respect to $\{\tilde{\boldsymbol{\theta}}_t, \tilde{\boldsymbol{\theta}}_r\}$ is given by

$$\min_{\tilde{\boldsymbol{\theta}}_t, \tilde{\boldsymbol{\theta}}_r} \quad \sum_{i \in \{t, r\}} \|\tilde{\boldsymbol{\theta}}_i - \boldsymbol{\theta}_i + \rho\tilde{\lambda}_i\|_2^2 \quad (59a)$$

$$\text{s.t.} \quad (54c), (54d). \quad (59b)$$

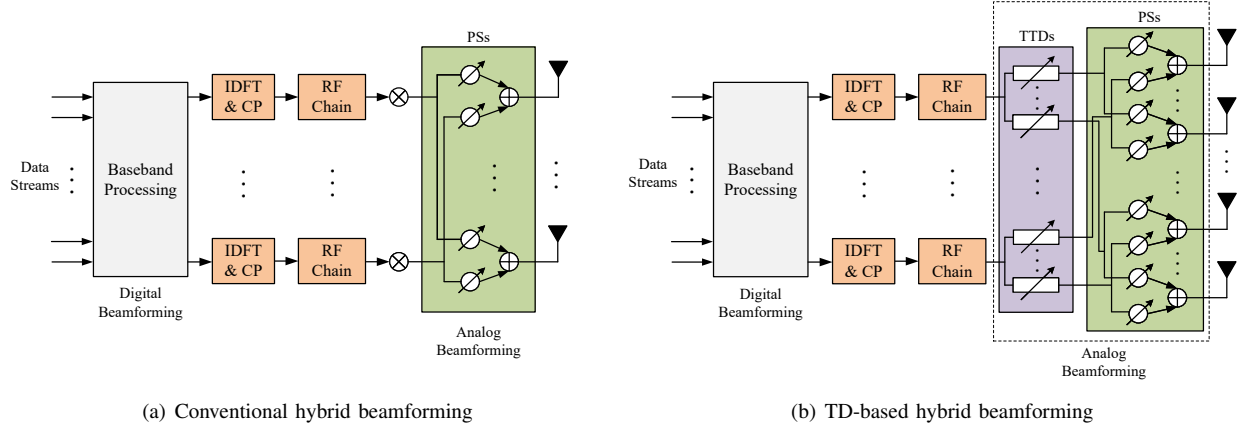


Fig. 4: Beamforming structures at the BS in wideband THz OFDM systems

Although this problem is non-convex due to the non-convex constraints, it has been shown in [32] that it can be solved by iteratively updating the amplitude vector $\tilde{\beta}_i \triangleq [\tilde{\beta}_{i,1}, \dots, \tilde{\beta}_{i,M}]^T, \forall i \in \{t, r\}$, and the phase-shift vector $\tilde{\phi}_i = [e^{j\tilde{\phi}_{i,1}}, \dots, e^{j\tilde{\phi}_{i,M}}]^T, \forall i \in \{t, r\}$. The closed-form optimal solutions for the phase-shift vector and the amplitude vector when the other is fixed have been given in [32, Proposition 1] and [32, Proposition 2], respectively, which is thus omitted here.

Finally, problem (54) can also be solved by exploiting the PDD framework. The corresponding algorithm has a similar structure as **Algorithm 2**. The differences with **Algorithm 2** are summarized as follows:

- The block $\{\theta_t, \theta_r\}$ is updated according to (58).
- The additional block $\{\tilde{\theta}_t, \tilde{\theta}_r\}$ is updated by iteratively updating $\{\beta_t, \beta_r\}$ and $\{\phi_t, \phi_r\}$.
- The new constraint violation function is defined as

$$\tilde{h} = \max \left\{ \begin{array}{l} \|\mathbf{F} - \mathbf{F}_{\text{RF}}\mathbf{F}_{\text{BB}}\|_{\infty}, \\ \max_{k,i} \|\xi_k - \mathbf{F}^T \mathbf{G}_k^T \theta_i\|_{\infty}, \\ \max_i \|\tilde{\theta}_i - \theta_i\|_{\infty} \end{array} \right\}. \quad (60)$$

- The additional dual variables $\{\tilde{\lambda}_t, \tilde{\lambda}_r\}$ are updated by

$$\tilde{\lambda}_i \leftarrow \tilde{\lambda}_i + \frac{1}{\rho}(\tilde{\theta}_i - \theta_i), \forall i \in \{t, r\}. \quad (61)$$

The initial point of the new PDD-based algorithm can be generated using the same method as that in the cases with independent phase-shift STARSs. Compared with **Algorithm 2**, the complexity of the new PDD-based algorithm mainly has differences in updating $\{\theta_t, \theta_r\}$ and $\{\tilde{\theta}_t, \tilde{\theta}_r\}$. Specifically, the complexity of updating according to (58) is $\mathcal{O}(M^3)$. The complexity of updating $\{\tilde{\theta}_t, \tilde{\theta}_r\}$ according to the closed-form solution in [32] is $\mathcal{O}(6M)$.

IV. WIDEBAND SYSTEM

In this section, we investigate the more challenging but more promising wideband STARS-aided THz OFDM system with the TD-based hybrid beamforming structure. The EE and SE maximization is also considered. In particular, we propose to

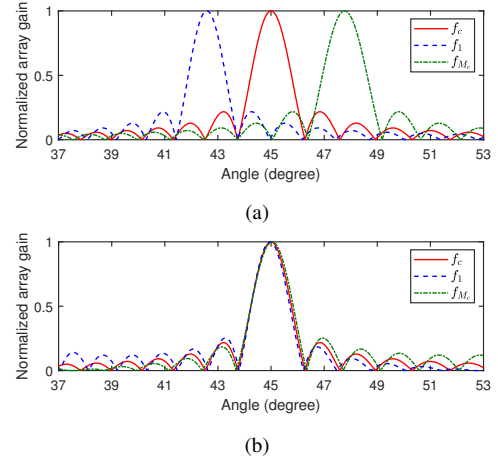


Fig. 5: Normalized array gain achieved by (a) the conventional hybrid beamforming and (b) the TD-based hybrid beamforming at different frequencies [16], where the desired physical direction is 45° , the central frequency is $f_c = 0.1$ THz, the system bandwidth is $W = 10$ GHz, and the number of subcarriers is $M_c = 10$.

solve the frequency-dependent phase shifts achieved by TTDs through the quasi-Newton method.

A. TD-based Hybrid Beamforming

Fig. 4(a) illustrates the conventional hybrid beamforming structure for wideband OFDM systems. In this structure, although different digital beamformers can be generated for different subcarriers with different frequencies, the analog beamformer can only be *frequency-independent* due to the hardware limitation of the PSs. In other words, all subcarriers share the same analog beamformer in the conventional hybrid beamforming structure. However, according to the analysis in Section II-C, the wideband THz channel can be significantly *frequency-dependent* due to the *frequency-dependent* array response vectors. Therefore, as shown in Fig. 5(a), the beams generated by the *frequency-independent* analog beamformer at each subcarrier will split into totally different physical directions, which is referred to as *beam split* effect. The beam

split effect can significantly degrade the array gain at different subcarriers, thus resulting in severe performance loss. As a remedy, the TD-based hybrid beamforming structure has been proposed recently [15], [16], as shown in Fig. 4(b). In this structure, a time-delay (TD) network realized by TTDs is added between the RF chains and the frequency-independent PSs. More specifically, each RF chain is connected to N PSs via N_T TTDs and each TTD is connected to $\frac{N}{N_T}$ PSs. Thus, there are $N_{\text{RF}}N_T$ TTDs and $N_{\text{RF}}N$ PSs in total. Unlike the PSs, the TTDs are capable of achieving *frequency-dependent* phase shifts. For example, a time delay t realized by the TTD becomes a $2\pi f_m t$ phase shift at the m -th subcarrier. Therefore, as shown in Fig. 5(b), the *frequency-dependent* analog beamforming can be jointly achieved by the TTDs and PSs to accommodate the significantly *frequency-dependent* wideband THz channels.

Denote $\bar{\mathbf{F}}_{\text{RF}} \in \mathbb{C}^{N \times N_T N_{\text{RF}}}$ as the analog beamformer achieved by the frequency-independent PSs, $\mathbf{T}_m \in \mathbb{C}^{N_T N_{\text{RF}} \times N_{\text{RF}}}$ as the frequency-dependent phase shifts achieved by TTDs, $\mathbf{F}_{\text{BB},m} = [\mathbf{f}_{m,1}^{\text{BB}}, \dots, \mathbf{f}_{m,K}^{\text{BB}}] \in \mathbb{C}^{N_{\text{RF}} \times K}$ as the digital beamformer for K user at m -th subcarrier, and $\mathbf{s}_m = [s_{m,1}, \dots, s_{m,K}]^T \in \mathbb{C}^{K \times 1}$ as the information symbols for K users at m -th subcarrier. More specifically, $\bar{\mathbf{F}}_{\text{RF}} = [\bar{\mathbf{F}}_1^{\text{RF}}, \dots, \bar{\mathbf{F}}_{N_{\text{RF}}}^{\text{RF}}]$ with $\bar{\mathbf{F}}_\ell^{\text{RF}} = \text{blkdiag}([\mathbf{f}_{\ell,1}^{\text{RF}}, \dots, \mathbf{f}_{\ell,N_T}^{\text{RF}}]) \in \mathbb{C}^{N \times N_T}$ denoting the analog beamformer connected to the ℓ -th RF chain via TTDs and $\mathbf{f}_{\ell,n}^{\text{RF}} \in \mathbb{C}^{\frac{N}{N_T} \times 1}$ denoting the corresponding analog beamformer connected to the n -th TTD. Then, we denote Ω and Ω_0 as the sets of indices of all elements and all non-zero elements of $\bar{\mathbf{F}}_{\text{RF}}$, respectively. As such, $\bar{\mathbf{F}}_{\text{RF}}$ needs to satisfy the following constraint:

$$|[\bar{\mathbf{F}}_{\text{RF}}]_{i,j}| = 1, \forall (i,j) \in \Omega_0, \quad (62a)$$

$$[\bar{\mathbf{F}}_{\text{RF}}]_{i,j} = 0, \forall (i,j) \in \Omega \setminus \Omega_0. \quad (62b)$$

Furthermore, matrix \mathbf{T}_m can be expressed as

$$\mathbf{T}_m = \text{blkdiag}([e^{-j2\pi f_m \mathbf{t}_1}, \dots, e^{-j2\pi f_m \mathbf{t}_{N_{\text{RF}}}}]), \quad (63)$$

where $\mathbf{t}_\ell = [t_{\ell,1}, \dots, t_{\ell,N_T}]^T \in \mathbb{C}^{N_T \times 1}$ denotes the time delays realized by TTDs connected to the ℓ -th RF chain, where $t_{\ell,n} \geq 0$. It can be noted from (63) that the phase shifts of matrices \mathbf{T}_m and $\mathbf{T}_n, \forall n \neq m$ are coupled with each other since they are realized by the same set of delays. With the TD-based hybrid beamforming, the transmit signal of the BS at the m -th subcarrier is given by

$$\mathbf{x}_m = \bar{\mathbf{F}}_{\text{RF}} \mathbf{T}_m \mathbf{F}_m^{\text{BB}} \mathbf{s}_m = \bar{\mathbf{F}}_{\text{RF}} \mathbf{T}_m \sum_{k \in \mathcal{K}} \mathbf{f}_{m,k}^{\text{BB}} s_{m,k}. \quad (64)$$

By assuming that \mathbf{s}_m is the independent complex Gaussian signal, the covariance matrix of \mathbf{x}_m can be calculated as $\mathbf{Q}_m = \mathbb{E}[\mathbf{x}_m \mathbf{x}_m^H] = \bar{\mathbf{F}}_{\text{RF}} \mathbf{T}_m \mathbf{F}_m^{\text{BB}} (\bar{\mathbf{F}}_{\text{RF}} \mathbf{T}_m \mathbf{F}_m^{\text{BB}})^H$. Furthermore, the average power allocated to each subcarrier is assumed to be the same, i.e.,

$$\text{tr}(\mathbf{Q}_m) = \|\bar{\mathbf{F}}_{\text{RF}} \mathbf{T}_m \mathbf{F}_m^{\text{BB}}\|_F^2 \leq P_t/M_c, \forall m \in \mathcal{M}_c. \quad (65)$$

The received signal at m -th subcarrier for user $k, \forall k \in \mathcal{K}_i, i \in \{t, r\}$, is given by

$$y_{m,k} = \bar{\mathbf{h}}_{m,k} \mathbf{x}_m + n_{m,k} = \bar{\mathbf{h}}_{m,k} \bar{\mathbf{F}}_{\text{RF}} \mathbf{T}_m \sum_{k \in \mathcal{K}} \mathbf{f}_{m,k}^{\text{BB}} s_{m,k} + n_{m,k}$$

$$= \underbrace{\theta_i^T \mathbf{G}_{m,k} \bar{\mathbf{F}}_{\text{RF}} \mathbf{T}_m \mathbf{f}_{m,k}^{\text{BB}} s_{m,k}}_{\text{desired signal}} + \underbrace{\sum_{j \in \mathcal{K}, j \neq k} \theta_i^T \mathbf{G}_{m,k} \bar{\mathbf{F}}_{\text{RF}} \mathbf{T}_m \mathbf{f}_{m,j}^{\text{BB}} s_{j,k} + n_{m,k}}_{\text{inter-user interference}}, \quad (66)$$

where $\mathbf{n}_{m,k} \sim \mathcal{CN}(0, \sigma_{m,k}^2)$ is the additive complex Gaussian noise with $\sigma_{m,k}^2 = \sigma_0^2 \frac{W}{M_c}$ and $\mathbf{G}_{m,k} \in \mathbb{C}^{M \times N}$ is the cascaded channel from BS to user k at m -th subcarrier as follows:

$$\mathbf{G}_{m,k} = \sum_{q=0}^{Q_k-1} \sum_{j=1}^{L_k} \sum_{i=1}^L \tilde{\mathbf{h}}_{i,j,q}^k(f_m) e^{-\frac{j2\pi m q}{M_c}}, \quad (67)$$

$$\tilde{\mathbf{h}}_{i,j,q}^k = \alpha_i \tilde{\alpha}_{k,j} G_r G_t \text{sinc}(q - W(\tau_i + \tau_{k,j})) \times \text{diag}(\mathbf{a}^H(f, \theta_{k,j}^h, \theta_{k,j}^v) \mathbf{a}(f, \varphi_\ell^h, \varphi_\ell^v) \mathbf{b}^H(f, \tilde{\varphi}_\ell), \quad (68)$$

which is obtained according to (6) and (12).

B. Problem Formulation

According to (66), the achievable rate for user $k, \forall k \in \mathcal{K}_i, i \in \{t, r\}$, at m -th subcarrier is given by

$$R_{m,k} = \log_2 \left(1 + \frac{|\theta_i^T \mathbf{G}_{m,k} \bar{\mathbf{F}}_{\text{RF}} \mathbf{T}_m \mathbf{f}_{m,k}^{\text{BB}}|^2}{\sum_{j \in \mathcal{K}, j \neq k} |\theta_i^T \mathbf{G}_{m,k} \bar{\mathbf{F}}_{\text{RF}} \mathbf{T}_m \mathbf{f}_{m,j}^{\text{BB}}|^2 + \sigma_{m,k}^2} \right). \quad (69)$$

Thus, the SE of the wideband STARS-aided THz-OFDM system is given by

$$\bar{g}(\bar{\chi}) = \frac{1}{M_c + L_{\text{CP}}} \sum_{m \in \mathcal{M}_c} \sum_{k \in \mathcal{K}} R_{m,k}, \quad (70)$$

where $\bar{\chi} = \{\theta_t, \theta_r, \bar{\mathbf{F}}_{\text{RF}}, \{\mathbf{T}_m\}_{m \in \mathcal{M}_c}, \{\mathbf{F}_m^{\text{BB}}\}_{m \in \mathcal{M}_c}\}$ and $L_{\text{CP}} \geq \max_{k \in \mathcal{K}} \{Q_k\}$ denotes the length of the cyclic prefix of the OFDM system. Then, the rate-dependent power consumption can be modeled as follows:

$$\bar{P}(\bar{\chi}) = \sum_{m \in \mathcal{M}_c} \|\bar{\mathbf{F}}_{\text{RF}} \mathbf{T}_m \mathbf{F}_m^{\text{BB}}\|_F^2 + \xi \bar{g}(\bar{\chi}) + \bar{P}_c. \quad (71)$$

The rate-independent power consumption \bar{P}_c is given by

$$\bar{P}_c = P_{\text{BS}} + P_{\text{BB}} + N_{\text{RF}} P_{\text{RF}} + N_{\text{RF}} N_T P_{\text{TTD}} + N_{\text{RF}} N P_{\text{RS}} + P_{\text{STAR}} + K P_{\text{UE}}, \quad (72)$$

where P_{TTD} denotes the power consumption of one TTD. As such, the EE is given by

$$\bar{\eta}(\bar{\chi}) = \frac{\bar{g}(\bar{\chi})}{\bar{P}(\bar{\chi})} = \frac{\bar{g}(\bar{\chi})}{\sum_{m \in \mathcal{M}_c} \|\bar{\mathbf{F}}_{\text{RF}} \mathbf{T}_m \mathbf{F}_m^{\text{BB}}\|_F^2 + \xi \bar{g}(\bar{\chi}) + \bar{P}_c} \quad (73)$$

Following the path in Section III-B, the general optimization problem for both EE and SE maximization for the wideband STARS-aided THz OFDM system can be formulated as follows:

$$\max_{\bar{\chi}} \frac{\bar{g}(\bar{\chi})}{w(\sum_{m \in \mathcal{M}_c} \|\bar{\mathbf{F}}_{\text{RF}} \mathbf{T}_m \mathbf{F}_m^{\text{BB}}\|_F^2 + \xi \bar{g}(\bar{\chi})) + \bar{P}_c} \quad (74a)$$

$$\text{s.t.} \quad \|\bar{\mathbf{F}}_{\text{RF}} \mathbf{T}_m \mathbf{F}_m^{\text{BB}}\|_F^2 \leq P_t/M_c, \forall m \in \mathcal{M}_c, \quad (74b)$$

$$t_{\ell,n} \geq 0, \forall \ell = 1, \dots, N_{\text{RF}}, n = 1, \dots, N_T, \quad (74c)$$

$$(2) \text{ or } (3), (62a), (62b), (63). \quad (74d)$$

Compared to problem (24) for the narrowband system, problem (74) is more challenging due to the additional frequency-dependent phase-shift matrices $\mathbf{T}_m, \forall m \in \mathcal{M}_c$ with coupled phase shifts.

C. Proposed Solution for Independent Phase-shift STARSs

In this subsection, we propose a new PDD-based algorithm for solving problem (74) under constraint (2), with a particular focus on addressing the coupling among the frequency-dependent phase-shift matrices $\mathbf{T}_m, \forall m \in \mathcal{M}_c$. Firstly, following the path in Section III-C and defining the auxiliary variables $\bar{\eta}, \bar{a}, \bar{b}, \bar{\mathbf{F}}_m = [\bar{\mathbf{f}}_{m,1}, \dots, \bar{\mathbf{f}}_{m,K}] \in \mathbb{C}^{N \times K}$, $\bar{\mathbf{r}}_m = [\bar{r}_{m,1}, \dots, \bar{r}_{m,K}]^T$, $\bar{\boldsymbol{\Xi}}_m = [\bar{\boldsymbol{\xi}}_{m,1}, \dots, \bar{\boldsymbol{\xi}}_{m,K}]^T$, and $\bar{\boldsymbol{\xi}}_{m,k} = [\bar{\xi}_{k,1}, \dots, \bar{\xi}_{k,K}]^T, \forall m \in \mathcal{M}_c$, problem (74) under constraint (2) can be converted into the following equivalent form:

$$\max_{\{\bar{\mathbf{F}}_m, \bar{\boldsymbol{\Xi}}_m, \bar{\mathbf{r}}_m\}_{m \in \mathcal{M}_c}, \bar{\eta}, \bar{a}, \bar{b}} \bar{\eta} \quad (75a)$$

$$\text{s.t. } \bar{\eta} \leq \frac{\bar{a}^2}{\bar{b}}, \quad (75b)$$

$$(M_c + L_{CP})\bar{a}^2 \leq \sum_{m \in \mathcal{M}_c} \sum_{k \in \mathcal{K}} \bar{r}_{m,k}, \quad (75c)$$

$$w \left(\sum_{m \in \mathcal{M}_c} \|\bar{\mathbf{F}}_m\|_F^2 + \frac{\xi \sum_{m \in \mathcal{M}_c} \sum_{k \in \mathcal{K}} \bar{r}_{m,k}}{M_c + L_{CP}} \right) + \bar{P}_c \leq \bar{b}, \quad (75d)$$

$$\bar{r}_{m,k} \leq R_{m,k}(\bar{\boldsymbol{\xi}}_{m,k}), \forall m \in \mathcal{M}_c, k \in \mathcal{K}, \quad (75e)$$

$$\|\bar{\mathbf{F}}_m\|_F^2 \leq P_t/M_c, \forall m \in \mathcal{M}_c, \quad (75f)$$

$$\bar{\mathbf{F}}_m = \bar{\mathbf{F}}_{\text{RF}} \mathbf{T}_m \mathbf{F}_m^{\text{BB}}, \forall m \in \mathcal{M}_c, \quad (75g)$$

$$\bar{\boldsymbol{\xi}}_{k,j}^m = \bar{\mathbf{F}}_m^T \mathbf{G}_{m,k}^T \boldsymbol{\theta}_i, \forall m \in \mathcal{M}_c, k \in \mathcal{K}_i, i \in \{t, r\}, \quad (75h)$$

$$(2), (62a), (62b), (63), (74c). \quad (75i)$$

where $R_{m,k}(\bar{\boldsymbol{\xi}}_{m,k})$ is defined as

$$R_{m,k}(\bar{\boldsymbol{\xi}}_{m,k}) = \log_2 \left(1 + \frac{|\bar{\xi}_{k,k}^m|^2}{\sum_{j \in \mathcal{K}, j \neq k} |\bar{\xi}_{k,j}^m|^2 + \sigma_{m,k}^2} \right). \quad (76)$$

Then, by introducing the dual variables $\bar{\Psi}_m$ and $\bar{\lambda}_{m,k}, \forall m \in \mathcal{M}_c, k \in \mathcal{K}$, for constraints (75g) and (75h), respectively, the following AL problem of problem (75) can be obtained:

$$\begin{aligned} \max_{\{\bar{\mathbf{F}}_m, \bar{\boldsymbol{\Xi}}_m, \bar{\mathbf{r}}_m\}_{m \in \mathcal{M}_c}, \bar{\eta}, \bar{a}, \bar{b}} \quad & \bar{\eta} - \sum_{m \in \mathcal{M}_c} \frac{1}{2\rho} \|\bar{\mathbf{F}}_m - \bar{\mathbf{F}}_{\text{RF}} \mathbf{T}_m \mathbf{F}_m^{\text{BB}} + \rho \bar{\Psi}_m\|_F^2 \\ & - \sum_{m \in \mathcal{M}_c} \sum_{i \in \{t, r\}} \sum_{k \in \mathcal{K}_i} \frac{1}{2\rho} \|\bar{\boldsymbol{\xi}}_{k,j}^m - \bar{\mathbf{F}}_m^T \mathbf{G}_{m,k}^T \boldsymbol{\theta}_i + \rho \bar{\lambda}_{m,k}\|_2^2 \end{aligned} \quad (77a)$$

$$\text{s.t. } (2), (62a), (62b), (63), (74c), (75b) - (75f). \quad (77b)$$

To solve the above AL problem, we divide the optimization variable into five blocks, namely $\{\{\bar{\mathbf{F}}_m, \bar{\boldsymbol{\Xi}}_m, \bar{\mathbf{r}}_m\}_{m \in \mathcal{M}_c}, \bar{\eta}, \bar{a}, \bar{b}\}, \{\boldsymbol{\theta}_t, \boldsymbol{\theta}_r\}, \bar{\mathbf{F}}_{\text{RF}}, \{\mathbf{F}_m^{\text{BB}}\}_{m \in \mathcal{M}_c}$, and $\{\mathbf{T}_m\}_{m \in \mathcal{M}_c}$. It can be readily seen that the subproblems with respect to the first four blocks have the same structure as the corresponding subproblems in the narrowband cases,

which can be solved by the same methods proposed in Section III-C. In the sequel, we propose to solve the subproblem with respect to the block $\{\mathbf{T}_m\}_{m \in \mathcal{M}_c}$ through the quasi-Newton method.

1) *Subproblem with respect to $\{\mathbf{T}_m\}_{m \in \mathcal{M}_c}$* : The block $\{\mathbf{T}_m\}_{m \in \mathcal{M}_c}$ only appears in the second term of the objective function and the constraints (63) and (74c). Thus, the corresponding subproblem is given by

$$\min_{\{\mathbf{T}_m\}_{m \in \mathcal{M}_c}} \sum_{m \in \mathcal{M}_c} \|\bar{\mathbf{F}}_m - \bar{\mathbf{F}}_{\text{RF}} \mathbf{T}_m \mathbf{F}_m^{\text{BB}} + \rho \bar{\Psi}_m\|_F^2 \quad (78a)$$

$$\text{s.t. } (63), (74c). \quad (78b)$$

With some algebraic manipulations, the above problem can be reformulated as follows:

$$\min_{\{\mathbf{T}_m\}_{m \in \mathcal{M}_c}} \sum_{m \in \mathcal{M}_c} \text{tr}((\mathbf{T}_m)^H \mathbf{C} \mathbf{T}_m \mathbf{D}_m) - 2\text{Re}\{\text{tr}(\mathbf{T}_m^H \mathbf{E}_m)\} \quad (79a)$$

$$\text{s.t. } (63), (74c), \quad (79b)$$

where $\mathbf{C} = \bar{\mathbf{F}}_{\text{RF}}^H \bar{\mathbf{F}}_{\text{RF}}$, $\mathbf{D}_m = \mathbf{F}_m^{\text{BB}} (\mathbf{F}_m^{\text{BB}})^H$, and $\mathbf{E}_m = \bar{\mathbf{F}}_{\text{RF}}^H (\bar{\mathbf{F}}_m + \rho \bar{\Psi}_m) (\mathbf{F}_m^{\text{BB}})^H$. The above problem can be transformed into an unconstrained optimization problem. Specifically, the objective function can be rephrased as a function of $t_{l,n}$ by substituting (63). Then, according to (63), $\mathbf{T}_m, \forall m \in \mathcal{M}_c$ are periodic function of $t_{l,n}$ with the periods $1/f_m, \forall m \in \mathcal{M}_c$, respectively. Typically, the ratio of these periods is rational, which implies that the objective function is also a periodic function of $t_{l,n}$. As such, for any negative $t_{l,n}$, we can always find a positive $t'_{l,n}$ that achieves the same objective value. Thus, constraint (74c) can be safely dropped. Now, since there is no constraint on $t_{l,n}$, problem (79) becomes an unconstrained optimization problem with respect to $t_{l,n}$. The new optimization variables $t_{l,n}$ can be directly optimized via the quasi-Newton method. Then, a stationary point of problem (79) can be obtained by substituting the optimized $t_{l,n}$ into (63). The total number of unconstrained optimization variables $t_{l,n}$ is the number of TTDs, i.e., $N_{\text{RF}} N_{\text{T}}$. Thus, by using the quasi-Newton method with Broyden-Fletcher-Goldfarb-Shanno (BFGS) formula for updating the approximation of the Hessian matrix, the complexity of each iteration is $\mathcal{O}(N_{\text{RF}}^2 N_{\text{T}}^2)$ [33].

Similarly, problem (75) can be solved via PDD. In the inner loop, the blocks $\{\{\bar{\mathbf{F}}_m, \bar{\boldsymbol{\Xi}}_m, \bar{\mathbf{r}}_m\}_{m \in \mathcal{M}_c}, \bar{\eta}, \bar{a}, \bar{b}\}, \{\boldsymbol{\theta}_t, \boldsymbol{\theta}_r\}, \bar{\mathbf{F}}_{\text{RF}}, \{\mathbf{F}_m^{\text{BB}}\}_{m \in \mathcal{M}_c}$, and $\{\mathbf{T}_m\}_{m \in \mathcal{M}_c}$ are updated iteratively. In the outer loop, the penalty factor and dual variables are updated. The initial optimization variables of the PDD are generated as follows. Firstly, to initialize $\bar{\mathbf{F}}_{\text{RF}}$ and $\mathbf{T}_m, \forall m \in \mathcal{M}_c$, the N_{RF} strongest paths are selected from the total L paths between the BS and the STARS. Then, they are initialized following the design principle proposed in [16]. More specifically, given the ℓ -th strong path with direction $\tilde{\phi}_\ell$, the ℓ -th component $\mathbf{F}_\ell^{\text{RF,init}} = \text{blkdiag}([\mathbf{f}_{\ell,1}^{\text{RF,init}}, \dots, \mathbf{f}_{\ell,N_{\text{T}}}^{\text{RF,init}}])$ of the initial frequency-independent analog beamformer is generated such that [16, Eq. (30)]

$$(\mathbf{f}_{\ell,n}^{\text{RF,init}})^T = e^{j\pi(n-1)P \sin \tilde{\phi}_\ell} [\mathbf{b}(f_c, \tilde{\phi}_\ell)]_{(n-1)P+1:nP}, \quad \forall n = 1, \dots, N_{\text{T}}. \quad (80)$$

TABLE I: System Parameters

N	The number of the BS antennas	128	L	The number of paths from BS to the STARS	4
N_{RF}	The number of the RF chains	4	L_k	The number of paths from STARS to user k	1
N_T	The number of the TTDs in the wideband system	8	W_n	Bandwidth for the narrowband system	10 MHz
M	The number of the STARS elements	20 ~ 100	W_w	Bandwidth for the wideband system	10 GHz
K	The number of users	4	M_c	The number of subcarriers in the wideband system	10
P_t	The maximum transmit power of the BS	-10 ~ 20 dBW	L_{CP}	The length of cyclic prefix in the wideband system	4
$k(f)$	Absorption coefficient	0.0033 m ⁻¹	G_t, G_r	The antenna gain at the BS and users	25 dBi, 15 dBi
σ_0^2	Noise power spectral density	-174 dBm/Hz			

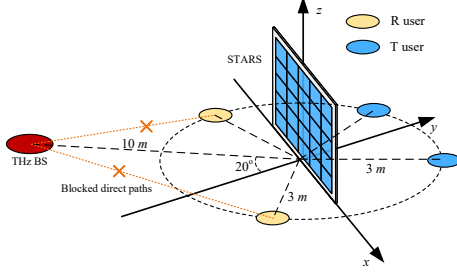


Fig. 6: The simulation setup.

where $P = N/N_T$. Then, for \mathbf{T}_m , the time delay for the n -th TTD connected to the ℓ -th RF chain is initialized as [16, Eq. (31)]

$$t_{\ell,n}^{\text{init}} = \begin{cases} (n-1) \frac{P \sin \tilde{\phi}_\ell}{2f_c}, & \sin \tilde{\phi}_\ell \geq 0, \\ (n-1) \frac{P \sin \tilde{\phi}_\ell}{2f_c} + (N_T - 1) \left| \frac{P \sin \tilde{\phi}_\ell}{2f_c} \right|, & \sin \tilde{\phi}_\ell < 0. \end{cases} \quad (81)$$

Then, the digital beamformers $\mathbf{F}_{\text{BB},m}, \forall m \in \mathcal{M}_c$ and the STARS coefficients $\{\theta_t, \theta_r\}$ are randomly initialized such that the constraint (74b) and the constraint (2) are satisfied, respectively. The auxiliary variables are initialized such that the corresponding equality constraints are satisfied.

D. Proposed Solution for Coupled Phase-shift STARSs

The solution for coupled phase-shift STARSs can be obtained by extending the solution for independent phase-shift STARSs based on the same method in Section III-D. Thus, we omit it here.

V. NUMERICAL RESULTS

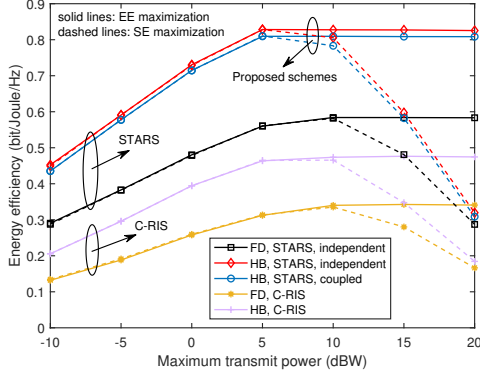
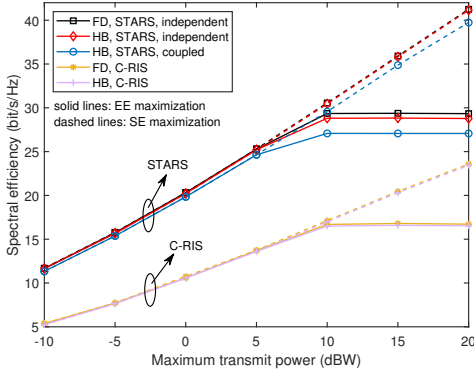
In this section, the numerical results obtained through Monte Carlo simulations are provided to evaluate the performance of the proposed STARS-aided THz wireless communication system in both narrowband and wideband cases. Fig. 6 illustrates the considered three-dimensional simulation setup. In particular, we assume the BS is 10 meters (m), under an angle of 20°, away from the STARS. The users are located on half-circles centered at the STARS with a radius of 3 m. The main adopted system parameters for the narrowband and wideband systems are given in Table I. The azimuth and elevation physical angles of the channel paths are randomly generated following $\mathcal{U}[-\frac{\pi}{2}, \frac{\pi}{2}]$. For the power consumption, the rate-dependent consumption factor ξ is set as 0.1 W/(bit/s/Hz). In the rate-independent power consumption, the practice values

are adopted as $P_{\text{BS}} = 3$ W [31], $P_{\text{BB}} = 300$ mW [34], $P_{\text{RF}} = 200$ mW [16], $P_{\text{PS}} = 30$ mW [34], $P_{\text{TTD}} = 100$ mW [35], and $P_{\text{UE}} = 100$ mW [31]. Regarding the power consumption of the STARS, we assume that the maximum tolerable error of the amplitudes and phase shifts are 0.005 and 1°, respectively. Thus, according to the model proposed in Section II-B, the power consumption of each element of the independent phase-shift STARS and the coupled phase-shift STARS are $\frac{1}{2} \left[\log_2 \frac{1}{0.005 \times 2} + 2 \log_2 \frac{360^\circ}{1^\circ \times 2} \right] \cdot P_{\text{PIN}} = 3.63$ mW and $\frac{1}{2} \left[\log_2 \frac{1}{0.005 \times 2} + \log_2 \frac{360^\circ}{1^\circ \times 2} + 1 \right] \cdot P_{\text{PIN}} = 2.64$ mW, respectively. Furthermore, for the conventional RIS (C-RIS) that can only transmit or reflect signals, the PIN diodes are only required to control the phase shifts. Thus, the power consumption of each element of the C-RIS is $\frac{1}{2} \left[\log_2 \frac{360^\circ}{1^\circ \times 2} \right] \cdot P_{\text{PIN}} = 1.32$ mW. For all the proposed algorithms, the convergence thresholds are set as 10^{-3} . The initial penalty factor of the PDD-based algorithms is set as $\rho = 10^4$ and its reduction factor is set as $c = 0.6$. All convex problems are solved by the CVX toolbox [36], and the quasi-Newton method is implemented by the fminunc in MATLAB. All results are obtained by averaging over 100 random channel realizations.

A. Narrowband System

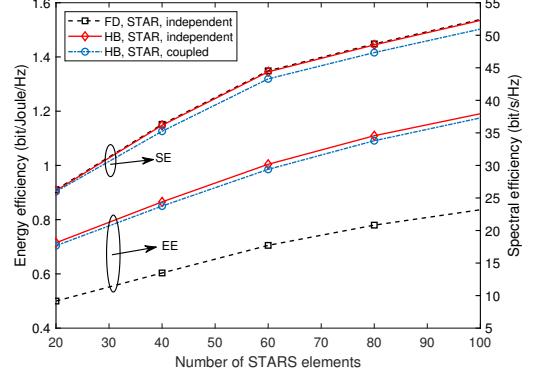
We first evaluate the performance of the proposed STAR-aided THz wireless communication system in the narrowband case and compare it with the following benchmark schemes: 1) **Full-digital (FD) beamforming**: In this scheme, each antenna at the BS is connected to an RF chain, which requires N RF chains. Thus, the transmit signal becomes $\mathbf{x}^{\text{FD}}[n] = \mathbf{F}_{\text{FD}} \mathbf{s}[n]$, where $\mathbf{F}_{\text{FD}} \in \mathbb{C}^{N \times K}$ is the FD beamformer; 2) **C-RIS**: In this scheme, there are two $\frac{M}{2}$ -element reflect-only and transmit-only RISs deployed adjacent to each other at the same place of the STARS.

1) *EE versus P_t* : In Fig. 7(a), we investigate the achieved EE under different maximum transmit power P_t using different schemes when $w = 1$ (EE maximization) and $w = 0$ (SE maximization). We set $M = 20$. For the results obtained by the EE maximization, it can be observed that the EE first increases with P_t and finally becomes constant. This is because the EE is not a monotonically increasing function of the transmit power P_t but has a finite upper bound. Actually, only a small part of the power is exploited for maximizing the EE when P_t is large. On the contrary, for SE maximization, although it achieves the same EE performance in the low-power region, it causes significant drops in the EE in the high-power region. This

(a) Energy efficiency versus P_t .(b) Spectral efficiency versus P_t .Fig. 7: Performance versus transmit power P_t for $M = 20$.

can be explained by the fact that the SE maximization always uses up all the achievable transmit power, which is not desired by the EE maximization. Furthermore, the proposed schemes with the STARS and the hybrid beamforming (HB) achieve the best performance compared to the benchmark schemes. On the one hand, STARSs always outperform C-RISs in terms of EE. The reasons behind this can be explained as follows. Since the STARS adopts all elements for both transmission and reflection, it is capable of generating finer directional beams toward users, resulting in higher array gain and better inter-user interference mitigation than the C-RIS. On the other hand, the HB always outperforms the FD. This is because, in the HB structure, a large number of RF chains with a large power consumption are replaced with a large number of PSs with much lower power consumption. Although these PSs cannot adjust the amplitude of signals as the RF chains, the HB structure can still achieve comparable SE as the FD structure, but uses much less power. Finally, it can also be seen that the performance of the coupled phase-shift STARS is close to that of the independent phase-shift STARS.

2) *SE versus P_t* : In Fig. 7(b), we investigate the achieved SE under different maximum transmit power P_t using different schemes when $w = 1$ (EE maximization) and $w = 0$ (SE maximization). We set $M = 20$. Fig 7(b) demonstrates a similar trend as Fig. 7(a), i.e., EE maximization and SE maximization are equivalent in the low-power region but becomes conflicting

Fig. 8: Performance versus the number of STARS elements M for $P_t = 10$ dBW.

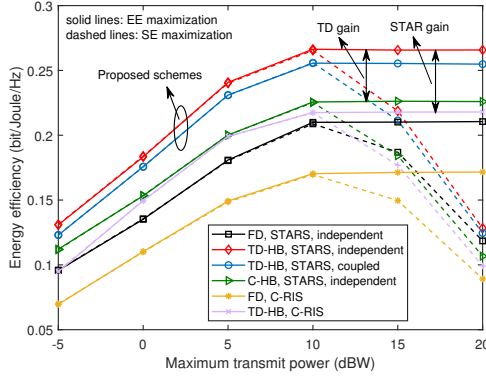
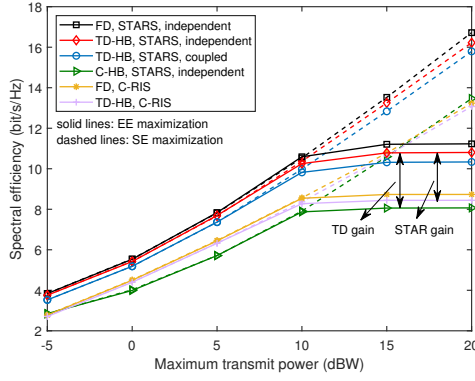
in the high-power region. More specifically, compared to the FD structure, there is only a slight performance loss caused by the HB structure, which further explains why the EE of the HB structure is much higher than that of the FD structure. Moreover, the plot of SE achieved by the STARS has a higher slope than that achieved by the C-RIS due to the more elements for both transmission and reflection in the STARS.

3) *EE & SE versus M* : In Fig. 8, we study the impact of the number of STARS elements on the maximum EE and SE. We set $P_t = 10$ dBW. As can be observed, both EE and SE monotonically increase with the number of RIS elements. This is because the larger number of STARS elements provides more degrees of freedom to achieve the higher SE but the power consumption introduced by the additional elements is relatively low.

B. Wideband System

In this subsection, the performance of the proposed schemes in the wideband OFDM system is evaluated, which is compared with the following benchmark schemes: 1) **FD beamforming**; 2) **C-RIS**; 3) **Conventional hybrid beamforming (C-HB)**: In this scheme, only the PSs are exploited to achieve the frequency-independent analog beamforming. Thus, the transmit signal at m -th subcarrier becomes $\mathbf{x}_m^{\text{C-HB}} = \bar{\mathbf{F}}_{\text{RF}}^{\text{C-HB}} \mathbf{F}_m^{\text{BB}} \mathbf{s}_m$, where $\bar{\mathbf{F}}_{\text{RF}}^{\text{C-HB}} \in \mathbb{C}^{N \times N_{\text{RF}}}$ is the frequency-independent analog beamformer with the constant modulus constraint.

1) *EE versus P_t* : In Fig. 9(a), we plot the EE versus the maximum transmit power P_t achieved by different schemes. We set $M = 20$. Firstly, we can also see the tradeoff between EE maximization and SE maximization in the high-power region. Furthermore, thanks to the frequency-dependent analog beamforming realized by the TTDs and the high degrees of freedom provided by the STARS, the proposed schemes achieve the best performance. In particular, compared to the C-HB structure, although the TD-based hybrid beamforming (TD-HB) structure introduces several additional TTDs that require much higher power consumption than the PSs, the frequency-dependent analog beamforming achieved by these TTDs eliminates the beam split effect in the wideband THz

(a) Energy efficiency versus P_t .(b) Spectral efficiency versus P_t .Fig. 9: Performance versus transmit power P_t for $M = 20$.

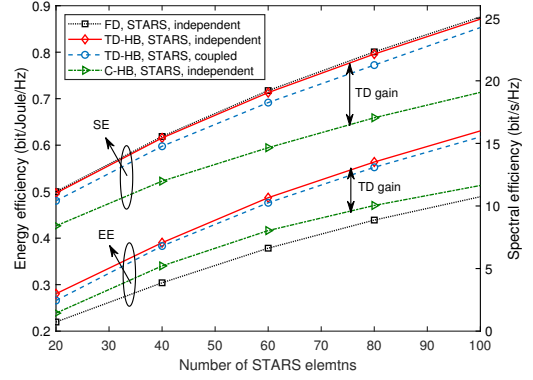
OFDM system, thus significantly enhancing the SE performance, which will be demonstrated in the following.

2) *SE versus P_t* : In Fig. 9(b), we plot the SE versus the maximum transmit power P_t achieved by different schemes. We set $M = 20$. As we can see, the TD-HB structure achieves comparable performance to the FD structure, while the C-HB structure causes significant performance loss in terms of SE due to the significant beam split effect. These results confirm the necessity of exploiting the TD-HB structure in the STARS-aided wideband THz OFDM system.

3) *EE & SE versus M* : In Fig. 10, we illustrate the maximum EE and SE versus the number of STARS elements. We set $P_t = 10$ dBW. Similarly, in the wideband OFDM system, the maximum EE and SE also increase with the number of STARS elements and the proposed schemes have the best performance.

VI. CONCLUSION

A STARS-aided THz communication system was proposed. Considering both independent and coupled phase shifts, the power consumption models were proposed for STARSs. The general EE and SE optimization problems were formulated for both narrowband and wideband systems to jointly design the hybrid beamforming and the STARS coefficients. In particular, a TD network was introduced into the hybrid beamforming structure to mitigate the beam split effect in the wideband

Fig. 10: Energy efficiency versus the number of STARS elements for $P_t = 10$ dBW.

system. The numerical results confirmed the effectiveness of exploiting the STARS with independent and coupled phase shifts in THz communications.

REFERENCES

- [1] Z. Zhang, Y. Xiao, Z. Ma, M. Xiao, Z. Ding, X. Lei, G. K. Karagiannidis, and P. Fan, "6G wireless networks: Vision, requirements, architecture, and key technologies," *IEEE Veh. Technol. Mag.*, vol. 14, no. 3, pp. 28–41, Sep. 2019.
- [2] I. F. Akyildiz, J. M. Jornet, and C. Han, "Terahertz band: Next frontier for wireless communications," *Phys. Commun.*, vol. 12, pp. 16–32, Sep. 2014.
- [3] I. F. Akyildiz, C. Han, Z. Hu, S. Nie, and J. M. Jornet, "Terahertz band communication: An old problem revisited and research directions for the next decade," *IEEE Trans. Commun.*, vol. 70, no. 6, pp. 4250–4285, Jun. 2022.
- [4] C. Huang, A. Zappone, G. C. Alexandropoulos, M. Debbah, and C. Yuen, "Reconfigurable intelligent surfaces for energy efficiency in wireless communication," *IEEE Trans. Wireless Commun.*, vol. 18, no. 8, pp. 4157–4170, Aug. 2019.
- [5] Y. Liu, X. Mu, J. Xu, R. Schober, Y. Hao, H. V. Poor, and L. Hanzo, "STAR: Simultaneous transmission and reflection for 360° coverage by intelligent surfaces," *IEEE Wireless Commun.*, vol. 28, no. 6, pp. 102–109, Dec. 2021.
- [6] X. Mu, Y. Liu, L. Guo, J. Lin, and R. Schober, "Simultaneously transmitting and reflecting (STAR) RIS aided wireless communications," *IEEE Trans. Wireless Commun.*, vol. 21, no. 5, pp. 3083–3098, May 2021.
- [7] C. Han, L. Yan, and J. Yuan, "Hybrid beamforming for terahertz wireless communications: Challenges, architectures, and open problems," *IEEE Wireless Commun.*, vol. 28, no. 4, pp. 198–204, Aug. 2021.
- [8] X. Yu, J.-C. Shen, J. Zhang, and K. B. Letaief, "Alternating minimization algorithms for hybrid precoding in millimeter wave MIMO systems," *IEEE J. Sel. Topics Signal Process.*, vol. 10, no. 3, pp. 485–500, Apr. 2016.
- [9] F. Sohrabi and W. Yu, "Hybrid digital and analog beamforming design for large-scale antenna arrays," *IEEE J. Sel. Topics Signal Process.*, vol. 10, no. 3, pp. 501–513, Apr. 2016.
- [10] W. Ni, X. Dong, and W.-S. Lu, "Near-optimal hybrid processing for massive MIMO systems via matrix decomposition," *IEEE Trans. Signal Process.*, vol. 65, no. 15, pp. 3922–3933, Aug. 2017.
- [11] G. Zhu, K. Huang, V. K. Lau, B. Xia, X. Li, and S. Zhang, "Hybrid beamforming via the kronecker decomposition for the millimeter-wave massive mimo systems," *IEEE J. Sel. Areas Commun.*, vol. 35, no. 9, pp. 2097–2114, Sep. 2017.
- [12] Q. Shi and M. Hong, "Spectral efficiency optimization for millimeter wave multiuser MIMO systems," *IEEE J. Sel. Topics Signal Process.*, vol. 12, no. 3, pp. 455–468, Jun. 2018.
- [13] H. Yuan, N. Yang, K. Yang, C. Han, and J. An, "Hybrid beamforming for terahertz multi-carrier systems over frequency selective fading," *IEEE Trans. Commun.*, vol. 68, no. 10, pp. 6186–6199, Oct. 2020.

- [14] H. Yuan, N. Yang, X. Ding, C. Han, K. Yang, and J. An, "Cluster-based multi-carrier hybrid beamforming for massive device terahertz communications," *IEEE Trans. Commun.*, vol. 70, no. 5, pp. 3407–3420, May 2022.
- [15] F. Gao, B. Wang, C. Xing, J. An, and G. Y. Li, "Wideband beamforming for hybrid massive MIMO terahertz communications," *IEEE J. Sel. Areas Commun.*, vol. 39, no. 6, pp. 1725–1740, Jun. 2021.
- [16] L. Dai, J. Tan, Z. Chen, and H. V. Poor, "Delay-phase precoding for wideband THz massive MIMO," *IEEE Trans. Wireless Commun.*, vol. 21, no. 9, pp. 7271–7286, Sep. 2022.
- [17] B. Ning, Z. Chen, W. Chen, Y. Du, and J. Fang, "Terahertz multi-user massive MIMO with intelligent reflecting surface: Beam training and hybrid beamforming," *IEEE Trans. Veh. Technol.*, vol. 70, no. 2, pp. 1376–1393, Feb. 2021.
- [18] W. Hao, G. Sun, M. Zeng, Z. Chu, Z. Zhu, O. A. Dobre, and P. Xiao, "Robust design for intelligent reflecting surface-assisted MIMO-OFDMA terahertz IoT networks," *IEEE Internet Thing J.*, vol. 8, no. 16, pp. 13 052–13 064, Aug. 2021.
- [19] Z. Wan, Z. Gao, F. Gao, M. Di Renzo, and M.-S. Alouini, "Terahertz massive MIMO with holographic reconfigurable intelligent surfaces," *IEEE Trans. Commun.*, vol. 69, no. 7, pp. 4732–4750, Jul. 2021.
- [20] W. Yan, W. Hao, C. Huang, G. Sun, O. Muta, and H. Gacanin, "Beamforming analysis and design for wideband THz reconfigurable intelligent surface communications," *arXiv preprint arXiv:2207.11926*, 2022.
- [21] Q. Shi and M. Hong, "Penalty dual decomposition method for non-smooth nonconvex optimization—part I: Algorithms and convergence analysis," *IEEE Transactions on Signal Processing*, vol. 68, pp. 4108–4122, Jun. 2020.
- [22] J. Xu, Y. Liu, X. Mu, and O. A. Dobre, "STAR-RISs: Simultaneous transmitting and reflecting reconfigurable intelligent surfaces," *IEEE Commun. Lett.*, vol. 25, no. 9, pp. 3134–3138, Sep. 2021.
- [23] J. Xu, Y. Liu, X. Mu, R. Schober, and H. V. Poor, "STAR-RISs: A correlated T&R phase-shift model and practical phase-shift configuration strategies," *IEEE J. Sel. Topics Signal Process.*, vol. 16, no. 5, pp. 1097–1111, Aug. 2022.
- [24] J. Xu, Y. Liu, X. Mu, J. T. Zhou, L. Song, H. V. Poor, and L. Hanzo, "Simultaneously transmitting and reflecting intelligent omni-surfaces: Modeling and implementation," *IEEE Veh. Technol. Mag.*, vol. 17, no. 2, pp. 46–54, 2022.
- [25] W. Tang, M. Z. Chen, X. Chen, J. Y. Dai, Y. Han, M. Di Renzo, Y. Zeng, S. Jin, Q. Cheng, and T. J. Cui, "Wireless communications with reconfigurable intelligent surface: Path loss modeling and experimental measurement," *IEEE Trans. Wireless Commun.*, vol. 20, no. 1, pp. 421–439, 2021.
- [26] D. Tse and P. Viswanath, *Fundamentals of wireless communication*. Cambridge, U.K.: Cambridge Univ. Press, 2005.
- [27] S. Priebe and T. Kurner, "Stochastic modeling of THz indoor radio channels," *IEEE Trans. Wireless Commun.*, vol. 12, no. 9, pp. 4445–4455, 2013.
- [28] T. S. Rappaport, Y. Xing, O. Kanhere, S. Ju, A. Madanayake, S. Mandal, A. Alkhateeb, and G. C. Trichopoulos, "Wireless communications and applications above 100 GHz: Opportunities and challenges for 6G and beyond," *IEEE Access*, vol. 7, pp. 78 729–78 757, Jun. 2019.
- [29] J. M. Jornet and I. F. Akyildiz, "Channel modeling and capacity analysis for electromagnetic wireless nanonetworks in the terahertz band," *IEEE Trans. Wireless Commun.*, vol. 10, no. 10, pp. 3211–3221, Oct. 2011.
- [30] Y. Liu, S. Zhang, F. Gao, J. Tang, and O. A. Dobre, "Cascaded channel estimation for RIS assisted mmwave MIMO transmissions," *IEEE Wireless Commun. Lett.*, vol. 10, no. 9, pp. 2065–2069, 2021.
- [31] E. Björnson, L. Sanguinetti, J. Hoydis, and M. Debbah, "Optimal design of energy-efficient multi-user MIMO systems: Is massive MIMO the answer?" *IEEE Trans. Wireless Commun.*, vol. 14, no. 6, pp. 3059–3075, Jun. 2015.
- [32] Z. Wang, X. Mu, Y. Liu, and R. Schober, "Coupled phase-shift STAR-RISs: A general optimization framework," *IEEE Wireless Commun. Lett.*, early access, Nov. 2, 2022, doi: 10.1109/LWC.2022.3219020.
- [33] J. Nocedal and S. Wright, *Numerical optimization*. New York, NY, USA: Springer-Verlag, 2006.
- [34] R. Méndez-Rial, C. Rusu, N. González-Prelcic, A. Alkhateeb, and R. W. Heath, "Hybrid MIMO architectures for millimeter wave communications: Phase shifters or switches?" *IEEE Access*, vol. 4, pp. 247–267, Jan. 2016.
- [35] M.-K. Cho, I. Song, and J. D. Cressler, "A true time delay-based SiGe bi-directional T/R chipset for large-scale wideband timed array antennas," in *Proc. IEEE Radio Freq. Integr. Circuits Symp. (RFIC)*, Philadelphia, PA, USA, Jun. 2018, pp. 272–275.
- [36] M. Grant and S. Boyd, "CVX: Matlab software for disciplined convex programming, version 2.1," <http://cvxr.com/cvx>, Mar. 2014.